

# Biophysical Analysis to Assess the Interaction of CRAC and CARC Motif Peptides of Alpha Hemolysin of *Escherichia coli* with Membranes

Lucía Cané, Fanny Guzmán, Galo Balatti, María Antonieta Daza Millone, Melisa Pucci Molineris, Sabina Maté, M. Florencia Martini, and Vanesa Herlax\*

Cite This: <https://doi.org/10.1021/acs.biochem.3c00164>

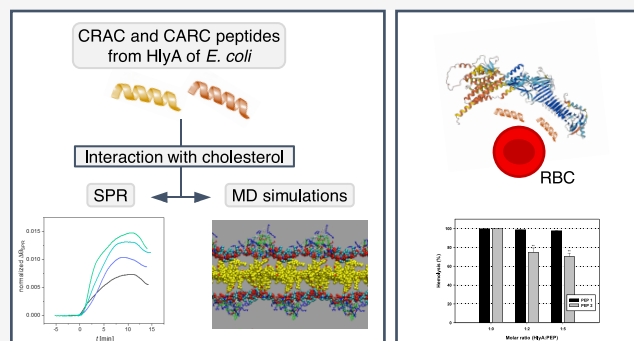
Read Online

ACCESS |

Metrics & More

Article Recommendations

**ABSTRACT:** Alpha hemolysin of *Escherichia coli* (HlyA) is a pore-forming protein, which is a prototype of the “Repeat in Toxins” (RTX) family. It was demonstrated that HlyA–cholesterol interaction facilitates the insertion of the toxin into membranes. Putative cholesterol-binding sites, called cholesterol recognition/amino acid consensus (CRAC), and CARC (analogous to CRAC but with the opposite orientation) were identified in the HlyA sequence. In this context, two peptides were synthesized, one derived from a CARC site from the insertion domain of the toxin (residues 341–353) (PEP 1) and the other one from a CRAC site from the domain between the acylated lysines (residues 639–644) (PEP 2), to study their role in the interaction of HlyA with membranes. The interaction of peptides with membranes of different lipid compositions (pure POPC and POPC/Cho of 4:1 and 2:1 molar ratios) was analyzed by surface plasmon resonance and molecular dynamics simulations. Results demonstrate that both peptides interact preferentially with Cho-containing membranes, although PEP 2 presents a lower  $K_D$  than PEP 1. Molecular dynamics simulation results indicate that the insertion and interaction of PEP 2 with Cho-containing membranes are more prominent than those caused by PEP 1. The hemolytic activity of HlyA in the presence of peptides indicates that PEP 2 was the only one that inhibits HlyA activity, interfering in the binding between the toxin and cholesterol.



## INTRODUCTION

Uropathogenic strains of *Escherichia coli* (UPEC), which cause 80% of the urinary tract infections (UTIs) in humans,<sup>1</sup> secrete a series of toxins.  $\alpha$ -Hemolysin (HlyA) is the virulence factor that correlates with the severity of the infections these bacteria produce.<sup>2,3</sup> UPEC can produce cystitis; pyelonephritis; and, in more severe cases, meningitis and septicemia.<sup>4</sup>

HlyA belongs to the RTX (Repeat in Toxins) family, whose structural characteristic gives the name to this family, and is a domain in the C-terminal end of the toxins. This domain consists of a variable number of glycine-rich and aspartate-containing nonapeptide repeats that bind calcium, which is an indispensable ion for toxin activity. Another important characteristic is that these toxins require a post-translational modification for activation, which involves a covalent amide linkage of two fatty acids to internal lysine (K) residues. Specifically, HlyA is acylated at K563 and K689.<sup>5–7</sup> This modification is not necessary for membrane binding or insertion, but it is crucial for lysis of the target cells.<sup>8–11</sup>

HlyA acts on a variety of cell types from different species, such as erythrocytes (RBC), fibroblasts, granulocytes,

lymphocytes, and macrophages,<sup>12–15</sup> and also binds to and disrupts protein-free liposomes.<sup>16</sup> The hemolytic mechanism of HlyA includes binding, insertion, and oligomerization of the toxin within the membrane, which ultimately leads to cell lysis.<sup>17,18,8,19</sup>

Concerning the insertion of the toxin into the membrane, it was demonstrated that residues 177 to 411 are the main region that participates in this event.<sup>20</sup> Furthermore, insertion is independent of membrane lysis because totally nonlytic mutants are also able to insert into the lipid monolayers.<sup>9</sup>

Once the toxin is inserted, oligomerization occurs. Fatty acids covalently bound to the toxin may produce the exposure of intrinsically disordered regions that promote protein–

Received: March 23, 2023

Revised: May 10, 2023

protein interaction.<sup>21,8</sup> Unfortunately, it was not possible to obtain an electron microscopy image or a crystal structure of the pore in the membrane; instead, upon characterization, the HlyA pore was proven to be of a proteolipidic nature because its conductance and membrane lifetime in black-lipid membrane experiments were found to depend on the membrane composition.<sup>22</sup> Moreover, it is a dynamic pore, and its size depends on both time and toxin concentration.<sup>23</sup> Regarding this, recently, we demonstrated that the interaction between HlyA and cholesterol (Cho) facilitates the insertion of the toxin into membranes in such a conformation that allows toxin oligomerization, which is necessary for pore formation.<sup>24</sup>

Putative Cho binding sites, called cholesterol recognition/amino acid consensus (CRAC) sites, have been identified in several proteins that interact with Cho.<sup>25,26</sup> The consensus sequence for the Cho-binding motif is in the N-terminus to C-terminus direction: L/V-(X<sub>1-5</sub>)-Y-(X<sub>1-5</sub>)-R/K, which consists of a branched apolar residue (L or V) followed by a variable segment containing from one to five residues of any amino acid, then the aromatic residue Y, then again one to five residues of any amino acid, and finally a basic residue (K or R).<sup>25,27</sup> Studying in more detail these Cho-binding motifs in specific domains of several proteins that interact with Cho, Baier *et al.* defined an inverted CRAC domain as "CARC".<sup>26</sup> The CARC motif K/R(X<sub>1-5</sub>)-Y/F-(X<sub>1-5</sub>)/L/V from the N- to C-terminus contains basic residues that ensure the correct position of the CARC motif at the polar/apolar interface of a transmembrane domain, exactly where Cho is supposed to be.<sup>26,27</sup>

A computational analysis demonstrated the presence of CRAC and CARC sites in the HlyA sequence.<sup>24</sup> Moreover, this Cho-binding motif has also been reported in other RTX toxins, suggesting that the interaction of toxins with Cho may be conserved in the entire toxin family.<sup>28</sup>

With the purpose of providing an understanding on the relationship between the structure and function of the toxin, in the present work, we synthesized two peptides. They correspond to a CARC region situated in the insertion domain of the toxin and a CRAC site situated between the acylated lysines. Their interaction with membranes of different compositions was studied by surface plasmon resonance (SPR). Molecular dynamics (MD) studies shed light on the interaction of the peptides with membranes at the molecular level. Finally, the hemolytic activity of the toxin in the presence of peptides was studied to comprehend the role of these sites in the mechanism of action of the toxin.

## MATERIAL AND METHODS

**Reagents and Materials.** 1-Palmitoyl-2-oleoyl-glycero-3-phosphocholine (POPC) and cholesterol (Cho) were purchased from Avanti Polar Lipids (Birmingham, AL, USA). DL-Dithiothreitol (DTT) was purchased from Sigma Aldrich (St. Louis, MO, USA). Chloroform and methanol (HPLC-grade) were purchased from Merck (Darmstadt, Germany). The ultrapure Milli Q water (Merck Millipore, Burlington, WI, USA) used for all the solutions and experiments had a resistivity of 18.2 MΩ cm at 23 °C. Glass substrates with gold evaporated (~50 nm) (SPR102-AU) were obtained from Bionavis (Tampere, Finland).

**Peptide Synthesis, Purification, and Characterization.** A CARC peptide of sequence RFKKLGYDGDSSL (341–353) (PEP 1) and a CRAC peptide of sequence VVYYDK (639–644) (PEP 2) were synthesized by solid-phase peptide

synthesis (SPPS) using the fluorenylmethoxycarbonyl protecting group (Fmoc) strategy.

First, 40 mg of Rink Amide resin was loaded onto polypropylene bags with *N,N*-dimethylformamide (DMF). Afterward, resin bags were washed in sequential steps with DMF, isopropyl alcohol (IPA), bromophenol blue (to assess for free amino groups), DMF, and finally dichloromethane (DCM). The coupling of the residues was performed using Fmoc amino acids, an activator, OxymaPure (ethyl cyanohydroxyiminoacetate), and *N,N*-diisopropylethylamine (DIEA) at 5/5/5/7.5 equiv, respectively. Activators used were *N*-[(1*H*-benzotriazol-1-yl)-(dimethylamino)methylene]-*N*-methylmethanaminium hexafluorophosphate *N*-oxide (HBTU) and (2-(1*H*-benzotriazol-1-yl)-1,1,3,3-tetramethyluronium hexafluorophosphate (TBTU) for single and double coupling, respectively. Cycles of removal of the Fmoc group and coupling of the next amino acid were performed until the sequence was completed. Peptide cleavage was done by the addition of 92.5% trifluoroacetic acid (TFA)/2.5% ultrapure water/2.5% triisopropylsilane. Finally, peptides were precipitated and washed with cold diethyl ether.

Peptides were subsequently purified using Clean-Up CEC18153 C-18 columns (UCT, Bristol, PA, USA) and eluted with an acetonitrile–water gradient from 0 to 70% (v/v). Fractions were analyzed by HPLC using a C18 column (Water Associates, Milford, MA, USA) and by ESI MS (Shimadzu 2020) mass spectrometry to confirm their molecular masses. The secondary structure of PEP 1 was determined by circular dichroism (CD) performed between 190 and 260 nm on a Jasco J-815 spectropolarimeter (Jasco Corp., Tokyo, Japan). Peptides were dissolved in phosphate-buffered saline (PBS) or in 30% 2,2,2-trifluoroethanol (TFE) for the measurements.

**Surface Plasmon Resonance Assays.** SPR substrates were modified to form a supported lipid bilayer (SLB) as previously described.<sup>29</sup>

**Vesicle Preparation.** Multilamellar vesicles (MLVs) of POPC and Cho were prepared by mixing the appropriate amounts of pure lipids dissolved in chloroform (1:0, 4:1, and 2:1). Samples were evaporated in a speed-vac (Speed Vac SC110, Savant) and hydrated in TC buffer (20 mM Tris and 150 mM NaCl (pH 7.4)). MLVs were sonicated for 1 h (TB04TA, Testlab, Argentina) to form small unilamellar vesicles (SUVs).

**DTT-Gold Substrate Preparation.** SPR gold substrates (BioNavis, Tampere, Finland) were washed with NH<sub>3</sub>/H<sub>2</sub>O<sub>2</sub>/H<sub>2</sub>O (1:1:2) at 90 °C for 5 min, rinsed with ultrapure water and absolute ethanol, and dried with N<sub>2</sub>. Immediately, substrates were immersed in a dithiothreitol (DTT) ethanolic solution (50 μM) for 30 min in the absence of light to achieve a fully covered surface with one monolayer of DTT.<sup>30</sup> Finally, substrates were rinsed with absolute ethanol and dried with a stream of N<sub>2</sub>.

**SPR Measurements.** SPR measurements were performed in Kretschmann configuration using a BioNavis Navi 200 (MP-SPR) device (Tampere, Finland) equipped with two independent lasers (670 and 785 nm) in a dual-channel system. Measurements were done in angular-scan mode (59–72°), with SPR curves recorded every 3.5 s at a constant temperature of 23 °C. *Ex situ* prepared DTT-gold substrates were placed in the flow chamber and washed with TC 10 mM CaCl<sub>2</sub> buffer (500 μL/min) and 1% Triton X-100 aqueous solution (1 min at 50 μL/min) before bilayer immobilization.

Vesicle suspensions (0.2 mg/mL) were injected at 10  $\mu\text{L}/\text{min}$  for 10 min for each specified composition. Unbound vesicles were washed with TC 10 mM  $\text{CaCl}_2$  buffer (500  $\mu\text{L}/\text{min}$ ) and 100 mM NaOH solution (1 min at 50  $\mu\text{L}/\text{min}$ ). The amount of immobilized lipid was recorded after 10 min of signal stabilization. For binding assays, it was injected peptides at different concentrations from 10 to 80  $\mu\text{M}$  in the TC buffer containing 10 mM  $\text{CaCl}_2$  for 10 min at 10  $\mu\text{L}/\text{min}$  on a fresh bilayer prepared for each binding assay (measurements were made at least by duplicate). Finally, DTT-gold surfaces were regenerated with two consecutive injections of 1% Triton X-100 aqueous solution (1 min at 50  $\mu\text{L}/\text{min}$ ) before a fresh vesicle suspension was injected. Figure 1 shows a representative sensogram obtained for each lipid composition. Numbers in the figure indicate the steps described above.

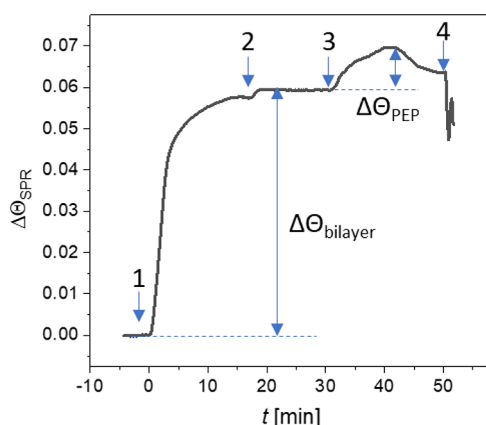


**Figure 1.** Representative sensogram of the SPR experiments. Plot of the change in minimum SPR angle ( $\Delta\Theta_{\text{SPR}}$ ) as a function of time. (1) Vesicle (0.2 mg/mL) injection, (2) washing step, (3) peptide injection, and (4) regeneration step. The values of  $\Delta\Theta_{\text{bilayer}}$  were used for normalizing the amount of immobilized lipid, and  $\Delta\Theta_{\text{PEP}}$  is the SPR signal at equilibrium for the peptide.

**Dissociation Constant ( $K_D$ ) Calculation.** The binding interaction between peptides and bilayers composed by pure POPC and POPC/Cho at 4:1 and 2:1 molar ratios was compared according to their calculated  $K_D$  values. The overall change in minimum SPR angle ( $\Delta\Theta_{\text{SPR}}$ ) was normalized considering the amount of immobilized lipid ( $\Delta\Theta_{\text{bilayer}}$ ) before each binding assay, and the total internal reflection (TIR) angle was subtracted for each association curve to remove the buffer contribution to SPR signal.

The relationship between the equilibrium binding response (Figure 1,  $\Delta\Theta_{\text{PEP}}$ ) and the peptide concentration ( $C$ ) can be described, among other approaches, by using a Langmuir binding model:<sup>31</sup>

$$\Delta\Theta_{\text{PEP}} = \Delta\Theta_{\text{PEP}(\text{max})} \times C / (K_D + C)$$

Then,  $K_D$  values were obtained by fitting  $\Delta\Theta_{\text{PEP}}$  vs  $C$  data (Origin software).

**Computer Setup for Molecular Dynamics (MD) Simulations.** MD simulations of bilayers composed of pure POPC and lipid mixtures of POPC/Cho (4:1 and 2:1 molar ratio) were performed in aqueous solution using the GROMACS 2020 software package.<sup>32–36</sup> POPC, Cho, and the peptide were described by the GROMOS-96 53a6 united atom force field<sup>34,35</sup> using the Berger *et al.* correction.<sup>37</sup> Water was modeled using the simple point charge (SPC) model.<sup>33</sup>

The systems were named SI, SII, and SIII for each model bilayer composed by pure POPC (1:0), POPC/Cho (4:1), and POPC/Cho (2:1), respectively. These membranes were simulated in the presence of 10 molecules of peptides PEP 1 (systems SXA, where X is I, II, or III) and PEP 2 (systems SXB, where X is I, II, or III) or in their absence to analyze the membrane behavior without a peptide (systems SXC, where X is I, II, or III) (Table 1). The simulated systems consist of a

**Table 1. Components of Each Simulated System<sup>a</sup>**

system name	POPC/Cho	peptide molecules
SIA	1:0	10 PEP1
SIIA	4:1	10 PEP1
SIIIA	2:1	10 PEP1
SIB	1:0	10 PEP2
SIIB	4:1	10 PEP2
SIIBB	2:1	10 PEP2
SIC	1:0	
SIIC	4:1	
SIICB	2:1	

<sup>a</sup>Number of peptide molecules and molar ratio of POPC/Cho for each simulated system.

periodically replicated cell of  $\sim 60 \times 60 \times 150 \text{ \AA}^3$ , containing 64 molecules of lipids in each leaflet (128 in total) and 10 molecules of peptides solvated with  $\sim 13,000$  molecules of water, and  $\text{Na}^+$ ,  $\text{Cl}^-$ , and  $\text{Ca}^{2+}$  ions to obtain 100 mM NaCl, 10 mM  $\text{CaCl}_2$ , and an electrically neutral system. The peptide and ion concentrations were the same as those used in SPR experiments to compare the peptide behavior.

The initial peptide structures (RFKKGVDGDSLL-NH<sub>2</sub> or VVYYDK-NH<sub>2</sub>) were taken from the predicted structures deposited in AlphaFold2<sup>38</sup> under the code P09983. The first sequence showed a “high” level of confidence, whereas the second one exhibited a “very high” level of confidence, as indicated by the per-residue estimate of its confidence score (pLDDT). Terminal K was manually edited to cap the peptide with an amide group to reproduce experimental conditions.

The electrostatic interactions were handled with the smooth particle mesh Ewald (SPME) version of the Ewald sums.<sup>39,40</sup> In all the simulations, the van der Waals and Coulombic interactions were cut off at 1.5 nm. Simulations were conducted in the NPT ensemble using the Nosé–Hoover thermostat. The entire system was coupled to a temperature bath with a reference temperature of 298 K in accordance with the experimental settings. The pressure was set at 1 bar using a Parrinello–Rahman barostat in a semi-isotropic perform with uniform scaling of  $x$ – $y$  axis independent of  $z$ . All bond lengths of the molecules were constrained using the LINCS algorithm. The time step for the integration of the equation of motion was 2 fs. Systems were minimized and equilibrated. MD simulations were carried out up to 200 ns production run after the equilibration of the system.

Simulated trajectories were analyzed visually with the VMD software, and snapshots of the most representative stages were obtained as well. For a quantitative analysis, the evaluated properties were examined with the tool package of the Gromacs software suite in different periods of the trajectory as reported in the Results section.

The figures of MD simulations were done with the VMD<sup>41</sup> and Grace (<http://plasma-gate.weizmann.ac.il/Grace/>) software.



**Protein and Mutant Protein Purification.** HlyA is a protein of 1023 amino acids devoid of cysteine. It was purified from culture filtrates of *E. coli* strain WAM 1824.<sup>42</sup> The HlyA cysteine mutant protein K344C (HlyA K344C) was purified from the *E. coli* strain WAM 2205.<sup>43</sup> All *E. coli* strains were kindly provided by Dr. R.A. Welch, University of Wisconsin, Madison, USA.

Proteins were purified following the protocol previously described.<sup>8</sup>

**Hemolytic Inhibition Assays.** *Ethics Statement.* Human blood was obtained from healthy volunteers from our laboratory staff, who gave the appropriate informed consent. The study was approved by the Committee of Bioethics and Ethics of Research of the School of Medical Sciences, National University of La Plata (UNLP) (Protocol No. 43) (COBIMED) [according to the requirements of the Declaration of Helsinki and the Argentine legislation concerning Public Health (laws No. 25326 and No. 26529)].

**Human Erythrocyte Isolation.** Erythrocytes were separated from the rest of the blood by centrifugation (1500g for 5 min), resuspended in the TC buffer, and washed three times. Finally, washed erythrocytes were diluted to the desired hematocrit.

**Hemolytic Inhibition Assays.** First, a 4% v/v erythrocyte suspension was preincubated with peptides at different concentrations for 30 min at 37 °C. Then, lytic concentration of HlyA was added (0.1 μM). HlyA/Peptide molar ratios assayed were 1:0, 1:2, and 1:5. The erythrocyte final concentration was 2% v/v.

The hemolytic activity was analyzed by measuring the decrease in light scattering at 595 nm of the erythrocyte suspension (2% v/v). The percent of hemolysis at 30 min was calculated using the following equation:

$$\% \text{Hemolysis} = (\text{OD}_0 - \text{OD}_x) \times 100 / (\text{OD}_0 - \text{OD}_{100}).$$

where the parameters OD<sub>0</sub>, OD<sub>x</sub>, and OD<sub>100</sub> correspond to the optical density of erythrocytes in the buffer and those treated with different concentrations of peptides and with Triton X-100, respectively.

**Binding Assays.** *Erythrocyte Membrane (Ghost) Preparation.* Packed human erythrocytes (1.5 mL) were washed with the TC buffer and then osmotically lysed in 10 mM Tris-HCl, pH 7.4 buffer, at 4 °C for 30 min. Membranes were pelleted (10 min at 14,500g) and washed with the TC buffer until the supernatant remained clear. Last, membranes were resuspended in 3 mL of the TC buffer.

**Binding to Ghost.** HlyA (180 pmol) was incubated with 75 μL of ghost for 1 h at 37 °C. Binding inhibition was studied following two preincubation approaches: (1) Ghost erythrocytes were preincubated with PEP 2 for 30 min at 37 °C, and then HlyA was added (180 pmol). (2) HlyA was first preincubated with PEP 2 for 30 min at 37 °C, and then ghost erythrocytes were added. The HlyA/PEP 2 molar ratio studied was 1:5. Later, membranes were separated by centrifugation at 10,000g for 10 min. The pellet was resuspended in a sampling buffer with 5% sodium dodecyl sulfate (SDS) and electrophoresed on a 10% SDS-PAGE. The gel was transferred to a PVDF membrane for 1 h at 100 V. Membranes were incubated with a blocking solution (3% skim milk in the TC buffer) and then with a polyclonal rabbit anti-HlyA antibody (1:500) or monoclonal mouse anti-β-actin (1:10,000) (A5316, Sigma). After several washes with the TC buffer, membranes were incubated with peroxidase conjugated secondary antibodies for 2 h. Finally, membranes were revealed

with a peroxidase substrate solution (ImmobilonWestern, Millipore), and images were obtained using the ChemiDoc MP Imaging System (Bio-Rad, Hercules, CA, USA).

**Fluorescence Resonance Energy Transfer (FRET) Assays.** Considering that the oligomerization process of HlyA was previously studied by measuring the efficiency of FRET between two populations of toxin labeled with a donor and acceptor fluorophore,<sup>8</sup> in the present work, these assays were repeated but in the presence of PEP 2.

**Labeling of HlyA K344C with Fluorescence Probes.** Considering that HlyA is devoid of Cys, an HlyA cysteine mutant protein K344C (HlyA K344C) was purified to ensure the labeling of the toxin with only one molecule of the fluorescent probe. The HlyA K344C in degassed TC buffer with 6 M GnHCl and 10 mM dTT (pH 7.4) was incubated overnight at 4 °C with sulfhydryl-specific probes. The fluorescent probes used were Alexa-488 (donor, D) and Alexa-546 (acceptor, A), added to a final molar ratio of 30:1 and 5:1 probe to protein, respectively. To label with Alexa-546, 0.1% sodium cholate was added. PD-10 columns (GE Healthcare) were used to separate labeled proteins from the unbound probe. The efficiency of labeling was determined from the molar extinction coefficients:  $\epsilon^{492} = 67,100 \text{ cm}^{-1} \text{ M}^{-1}$ ,  $\epsilon^{554} = 90,300 \text{ cm}^{-1} \text{ M}^{-1}$ , and  $\epsilon^{280} = 73,960 \text{ cm}^{-1} \text{ M}^{-1}$  for Alexa-488, Alexa-546, and HlyA, respectively. Labeled proteins maintained their hemolytic activity as the unlabeled ones. The toxin used was specifically labeled, with a molar ratio between 0.9 and 1.1 probe to protein.

**Interaction of Labeled HlyA K344C and HlyA K344C-PEP 2 with Ghosts.** For each experiment, three types of samples combining labeled and unlabeled HlyA K344C were measured: (a) D/unlabeled mutant protein, (b) D/A, and (c) unlabeled mutant protein/A, at 1:1 molar ratio. The protein (a, b, or c; 120 μg) was incubated with 75 μL of ghost (prepared as previously described) at 37 °C for 60 min in the TC buffer with 10 mM CaCl<sub>2</sub>. The resulting final reaction volume was 1 mL. Membranes were separated by centrifugation (10 min, 14,500g) and washed with TC to separate unbound protein. Finally, samples were resuspended in 200 μL of the same buffer.

For experiments in the presence of PEP 2, 75 μL of ghosts was preincubated with the peptide for 30 min at 37 °C, and then 120 μg of proteins (a, b, and c) was added. The protocol was the same as that for toxin only. The protein/peptide molar ratios studied were 1:5 and 1:10.

**FRET Measurements.** Fluorescence emission spectra were recorded at room temperature on a Fluorolog-3 Spectrofluorometer (Horiba-Jobin Yvon). Alexa-488 was excited at 480 nm, and emission was recorded between 500 and 650 nm. Direct excitation of Alexa-546 was achieved at 530 nm, and the emission was recorded between 540 and 650 nm.

The efficiency of energy transfer (*E*) was calculated as the enhancement of the acceptor fluorescence emission as described by Gohlke *et al.*<sup>44</sup> This method employs the fluorescence emission spectrum of erythrocyte membranes containing D/A excited at 480 nm ( $F_{480}^{(D/A)}$ ), which is fitted to the weighted sum of two emission spectra: one from erythrocyte membranes bound to labeled HlyA only with donor excited at 480 nm ( $F_{480}^D$ ) and the other from erythrocyte membranes containing D/A excited at 530 nm ( $F_{530}^{(D/A)}$ ), as shown in the following equation:

$$F_{480}^{(D/A)} = a \times F_{480}^D + b \times F_{530}^{(D/A)}$$



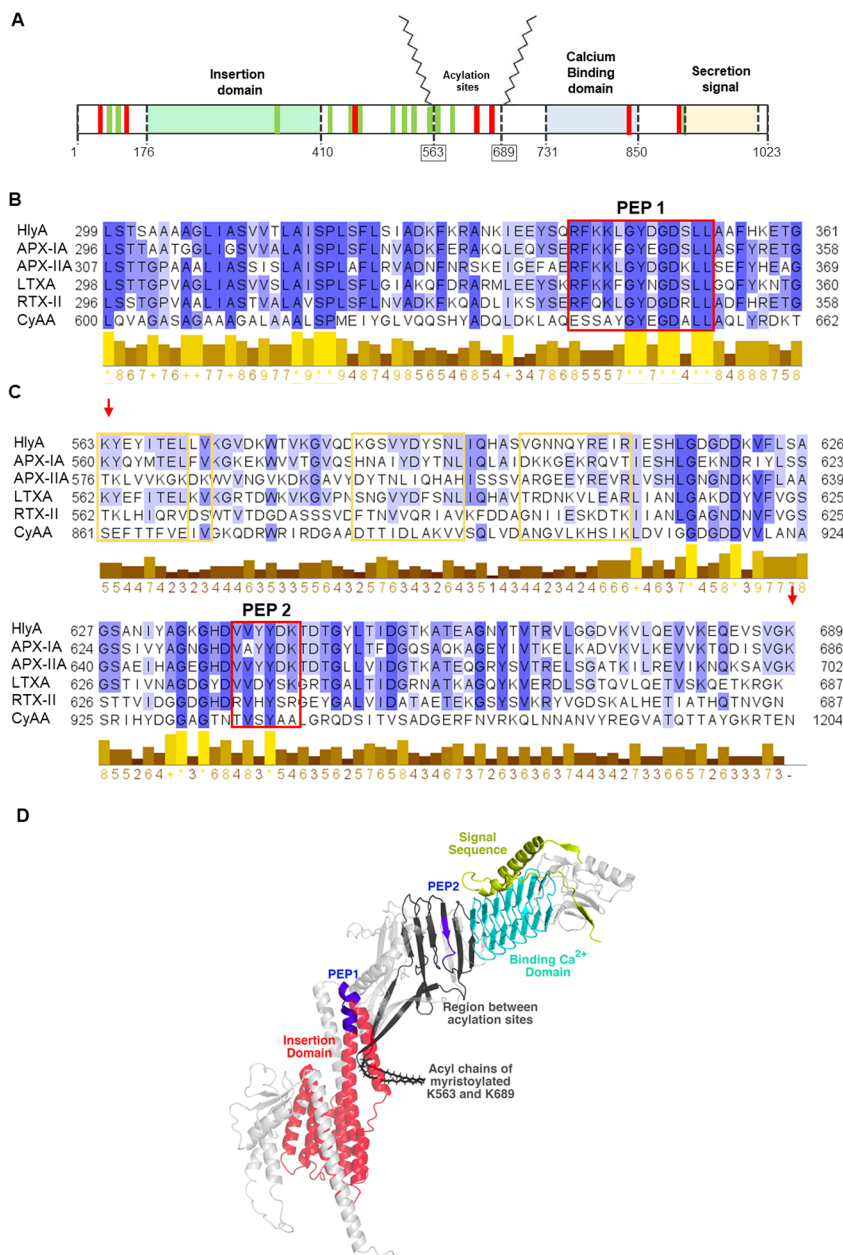


**Figure 2.** Multiple sequence alignment of different HlyA domains with other RTX toxins. (A) Toxin scheme where CARC sites are indicated in green and CRAC sites are in red considering results obtained by Vazquez *et al.*<sup>24</sup> (B) Alignment of the membrane insertion domain of HlyA and the CARC site corresponding to PEP 1 (green). (C) Alignment of the region between the acylated-Lys (red arrows) of HlyA, comprising the CRAC site corresponding to PEP 2 (red), and other CRAC/CARC sites (light). The sequences used for the alignment were the following: HlyA, *E. coli* (UniProtKB P09983); RTX-I, *A. pleuropneumoniae* (UniProtKB P55128); RTX-III, *A. pleuropneumoniae* (UniProtKB P55131); LtxA, *A. actinomycetemcomitans* (UniProtKB P16462); RTX-II, *A. pleuropneumoniae* (UniProtKB P15377); and CyaA, *B. pertussis* (UniProtKB J7QLCO). The alignment was performed with the ClustalW software,<sup>48</sup> and the image was created with the Jalview V2 software.<sup>49</sup> Residues were colored according to their percentage identity. (D) AlphaFold model of HlyA. The insertion domain of the toxin is colored in red, the region between the acylated-K is indicated in black, peptides are colored in blue, the binding calcium domain is colored in light blue, and the signal sequence for toxin exportation is in green.

The coefficients *a* and *b* are the fitted fractional contributions of the two spectral components; *b* is the acceptor fluorescence signal due to FRET from the donor, normalized by  $F_{530}^{(D/A)}$ . The fitting of the spectra was made using Sigmaplot 12.0 (Jandel Scientific, San Rafael, CA). Finally, *E* was obtained using the *b* value according to the following equation:

$$b = E \times (\epsilon^D(480))/(\epsilon^A(530)) + (\epsilon^A(480))/(\epsilon^A(530))$$

$\epsilon^D$  and  $\epsilon^A$  are the molar absorption coefficients of D and A at the given wavelengths. The absorption spectrum of membranes was subtracted in all the samples.

**Statistical Analysis.** A Student *t* test was used for statistical comparisons among groups, and differences were considered statistically significant when  $P < 0.05$  (\* $P < 0.05$ , \*\* $P < 0.01$ , and \*\*\* $P < 0.001$ ).

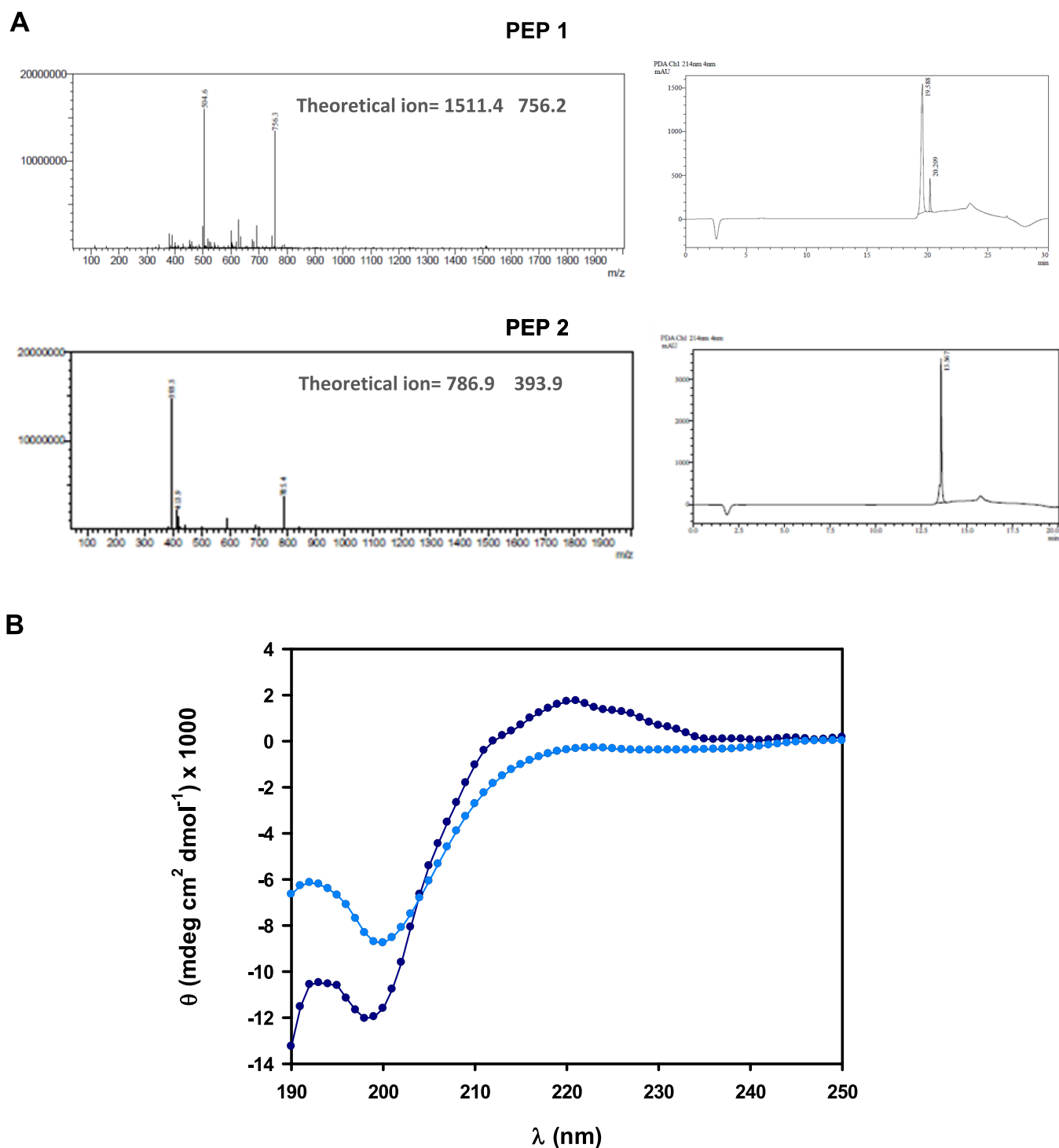


**Figure 3.** Peptide characterization. (A) Mass and HPLC chromatograms of PEP 1 and PEP 2. (B) CD spectrum of PEP 1 in PBS (dark blue) and in 30% TFE (light blue).

## RESULTS

### Peptide Synthesis and Biophysical Characterization.

Computational analyses revealed the presence of several CRAC and CARC sites in the HlyA sequence.<sup>24</sup> Figure 2A shows a scheme of the toxin where CARC regions are colored in green and CRAC regions are in red. Our previous results indicate that the interaction of the toxin with Cho might be implicated in the insertion of the toxin into membranes<sup>24</sup> or in the adoption of a competitive conformation for oligomeriza-

tion to occur.<sup>10</sup> In turn, in the present work, we studied CRAC and/or CARC regions situated in the insertion domain or in the region between the acylated-K. Only one CARC site is situated in the insertion domain of the toxin, so taking this into account, a peptide whose sequence corresponds to this CARC site (RFKKLGYDGDSSL) was synthesized (PEP 1). This site is highly conserved among the RTX toxins (Figure 2B).

On the other hand, two CARC and two CRAC sites are present in the domain between the acylated sites; therefore, a multiple sequence alignment between several RTX toxins

## PEP 1

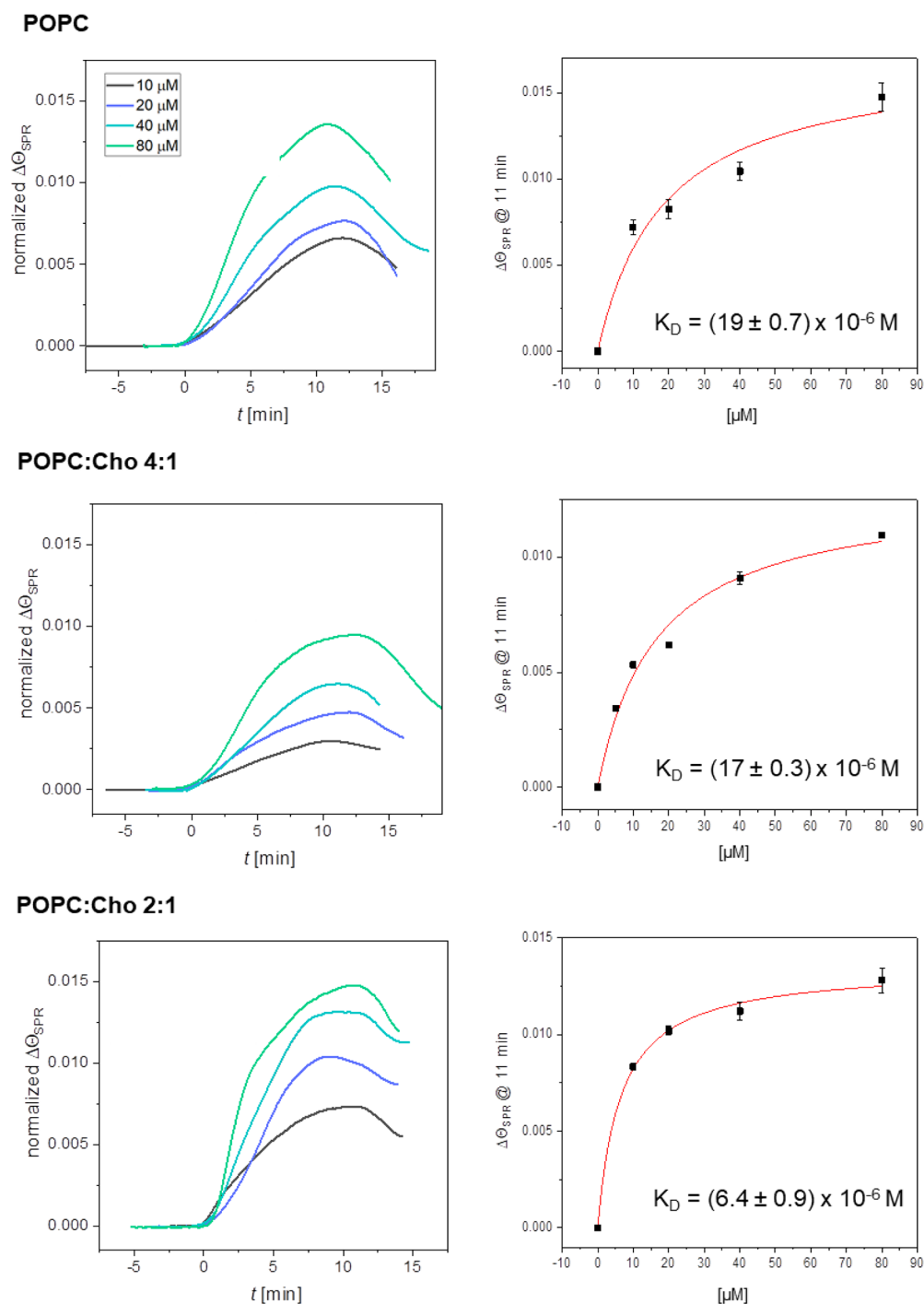


**Figure 4.** Interaction of PEP 1 with supported bilayers determined by SPR. (Left) Sensograms showing the interaction of different concentrations of PEP 1 (10–80  $\mu\text{M}$ ) with supported bilayers composed of POPC, 4:1 molar ratio POPC/Cho mixture, and 2:1 molar ratio of POPC/Cho mixture. The change in minimum SPR angle ( $\Delta\Theta_{\text{SPR}}$ ) was normalized considering the amount of immobilized lipid before each binding assay. For each PEP binding assay, the corresponding concentration of peptide in TC buffer containing 10 mM  $\text{CaCl}_2$  was injected ( $t = 0$ ) for 10 min at 10  $\mu\text{L}/\text{min}$ . (Right)  $\Delta\Theta_{\text{SPR}}$  at 11 min vs peptide concentration plots for the three lipid mixtures.  $K_D$  values were obtained from these plots as described in the Materials and Methods section ( $N = 2$ ).

(Figure 2C) was performed, and the region between amino acids 639 and 644 appeared highly conserved. In addition, previous results indicated that the deletion mutants HlyA  $\Delta 622$ –657 and HlyA  $\Delta 623$ –673 were cytotoxic and hemolytically inactive despite the fact that they were double

acylated.<sup>45,43</sup> This indicates the importance this region may have in the cytotoxic mechanism of the toxin. Then, a second peptide whose sequence is VVYYDK (639–644) was synthesized (PEP 2). Figure 2D shows an AlphaFold model of the toxin where the main domains are indicated. PEP 1 and



## PEP 2

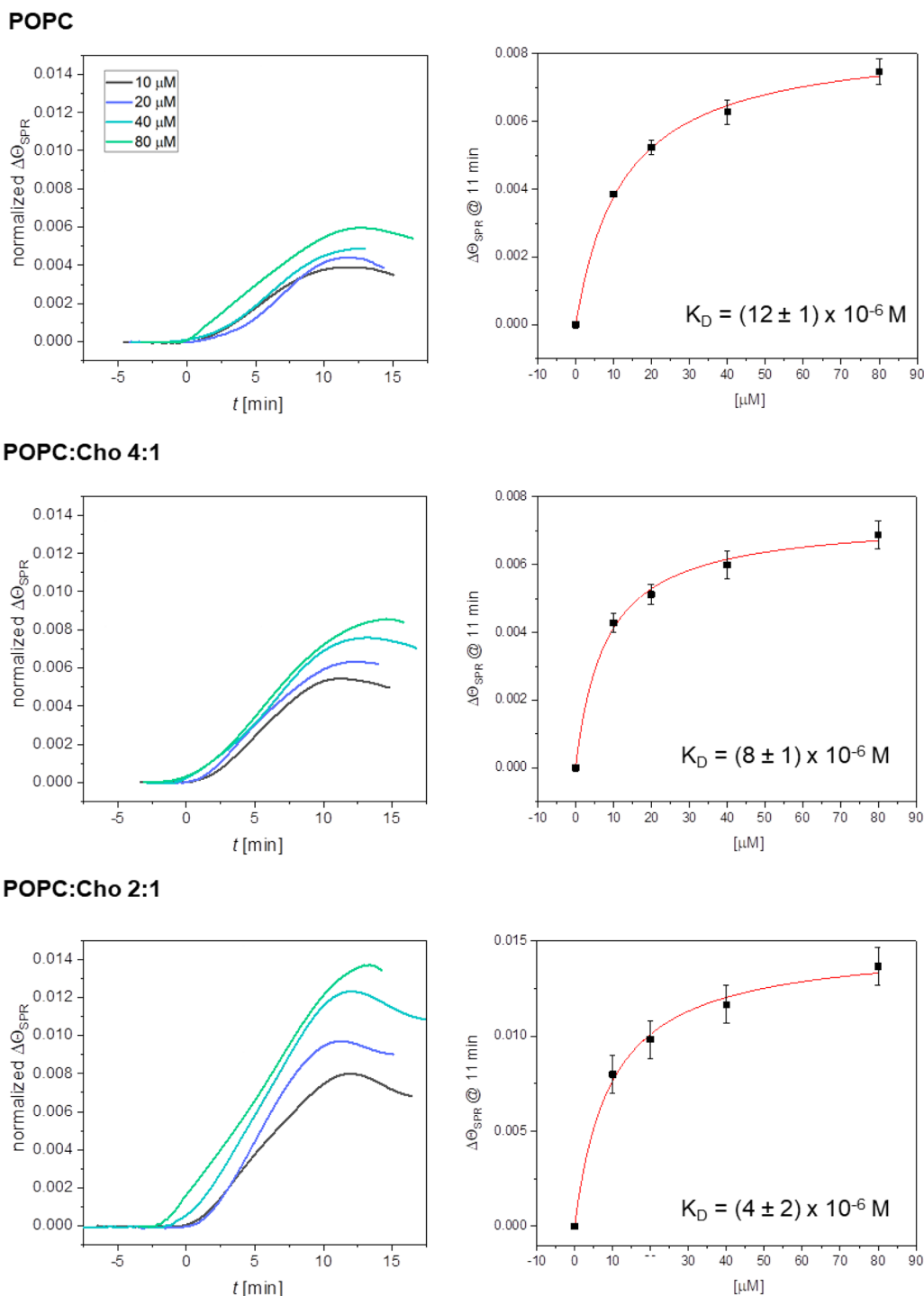


**Figure 5.** Interaction of PEP 2 with supported bilayers determined by SPR. (Left) Sensograms showing the interaction of different concentrations of PEP 2 (10–80  $\mu\text{M}$ ) with supported bilayers composed of POPC, 4:1 molar ratio POPC/Cho mixture, and 2:1 molar ratio of POPC/Cho mixture. The change in minimum SPR angle ( $\Delta\Theta_{\text{SPR}}$ ) was normalized considering the amount of immobilized lipid before each binding assay. For each PEP binding assay, the corresponding concentration of peptide in TC buffer containing 10 mM  $\text{CaCl}_2$  was injected ( $t = 0$ ) for 10 min at 10  $\mu\text{L}/\text{min}$ . (Right)  $\Delta\Theta_{\text{SPR}}$  at 11 min vs peptide concentration plots for the three lipid mixtures.  $K_D$  values were obtained from these plots as described in the Materials and Methods section ( $N = 2$ ).

PEP 2 are highlighted in the model to show their position within the possible conformation of the toxin in the solution.

Peptides were synthesized following the Fmoc-SPPS chemical synthesis approach,<sup>46</sup> as described in the Materials and Methods section. The molecular mass of the resulting

peptides was confirmed by mass spectrometry, which showed a clean product (Figure 3A). The conformational structure of PEP 1 in PBS (physiological condition) and 30% TFE (hydrophobic environment) was analyzed by CD. In the presence of PBS buffer, the peptide presented a polyproline II

structure, a more extended helix than the classical  $\alpha$ -helix. Because of this overextended conformation and high solvent exposure, residues within polyproline may lead to potential interaction with other molecular partners.<sup>47</sup> This structure was lost in 30% TFE (Figure 3B). CD of PEP 2 was not performed because of its short sequence.

**Study of Peptide Interaction with Bilayers Containing Different Amounts of Cholesterol by SPR.** Taking advantage of the SPR technique, the interaction of the peptides with supported lipid bilayers (SLBs) was studied. SLBs were formed by fusion of lipid vesicles of pure POPC or POPC/Cho lipid mixtures at 4:1 and 2:1 molar ratios on an SPR gold sensor chip covered with a DTT monolayer.<sup>29</sup> Figures 4 and 5 show the sensograms and the  $\Delta\Theta_{\text{PEP}}$  ( $\Delta\Theta_{\text{SPR}}$  at  $\sim 600$  s) vs peptide concentration plots obtained for each lipid composition for PEP 1 and PEP 2, respectively. Sensograms revealed that the signal intensity increased as a function of the peptide's concentration, indicating that the amount of peptide bound to the lipids is proportional to peptide concentration, although this effect is less notorious for the interaction between PEP 2 and POPC membranes. In this system, the signal is lower compared to the interaction with POPC/Cho 2:1 membranes. Then,  $K_D$  values were obtained by fitting  $\Delta\Theta_{\text{PEP}}$  at 11 min vs each peptide concentration for the interaction with the three different membrane compositions (4Figures 4 and 5). Figure 6

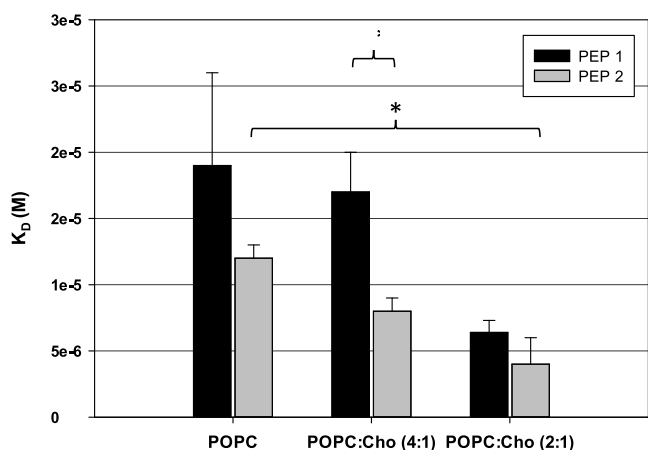


**Figure 6.**  $K_D$  values of PEP 1 and PEP 2. Bar plot of the  $K_D$  values of PEP 1 and PEP 2 with supported bilayers composed of POPC, 4:1 molar ratio of POPC/Cho mixture, and 2:1 molar ratio of POPC/Cho mixture.  $K_D$  values are those obtained from Figures 4 and 5.

shows a bar plot that compares the  $K_D$  values obtained for both peptides with different membranes. Results show that both peptides present more affinity for cholesterol-containing membranes. This preference is more notorious for PEP 2 than PEP 1. The  $K_D$  for PEP 2-POPC is three times higher compared to PEP 2-POPC/Cho 2:1. When comparing both peptides, results indicate that PEP 2 presents a higher affinity for membranes than PEP 1 in all the membranes tested.

#### MD Simulation of the Interaction of Peptides with Bilayers Containing Different Amounts of Cholesterol.

To study the interaction of the peptides with POPC/Cho bilayers (1:0, 4:1, or 2:1 molar ratios) from a molecular approach, MD simulations of these membrane compositions were performed in the presence (SIA, SIIA, and SIIIA systems for PEP 1; SIB, SIIB, and SIIIB systems for PEP 2) and absence (SIC, SIIC, and SIIIC systems) of peptides.

To compare the tendency of the peptides to interact or even insert into the interphase of the membrane, the mass density profile of the last 100 ns along the  $z$  axis of the simulated systems was calculated (Figure 7). Both peptides show a slight interaction with the membrane at the interphase level in the SI systems. PEP 2 penetrates the interphase more compared to PEP 1 because many PEP 1 molecules were also found throughout the aqueous region. Instead, in Cho-containing membranes, the density profile of both peptides shows their strong localization close to the bilayer surface, this effect being more evident for PEP 2 (SIIB and SIIIB systems) than for PEP 1 (SIIA and SIIIA systems). PEP 2 seems to insert deeper inside the Cho-containing membranes compared to PEP 1. This result agrees with the  $K_D$  calculated for both peptides with the different lipid bilayers (Figure 6).

When each peptide is analyzed separately, some differences are observed. PEP 1 penetrates more into the POPC/Cho 4:1 bilayer (SIIA system). The density profile of this peptide with the POPC/Cho 4:1 bilayer shows a deeper penetration of the peptide in the interphase region of the membrane of the SII system than of SIII, which generates an internalization of the polar groups of POPC toward the zone of the hydrocarbon tails. In these profiles, a redistribution of Cho is also observed. Cho migrates toward the center of the membrane, but the density profile of the central hydroxyl of the sterol is homogeneously distributed throughout the membrane profile (Figure 7, central panels). Instead, in the SIIIA system, although PEP 1 is localized in the interphase region, the lipid distribution observed in SIIA is not seen. This indicates the preference of PEP 1 for the POPC/Cho 4:1 bilayer.

On the other hand, PEP 2 penetrates both types of membranes (SII and SIII) (Figure 7, right panels), and the same lipid distribution described for SII in both systems for this peptide is observed. In addition, PEP 2 is localized deeper toward the center of the membrane compared to PEP 1. This last effect is also evidenced by the order parameter of the hydrocarbon tails of POPC calculated for the different membrane systems in the presence of both peptides. Figure 8A shows that PEP 2 penetrates deeper into the membrane because it modifies the order parameter up to carbon 6 of the palmitoyl chain and carbon 9 of the oleoyl chain of the POPC molecules. The most evident change in the order parameter is observed in SIII. Instead, PEP 1 only alters slightly the order parameter of the palmitoyl chain, up to carbon 2.

Taking into account the relevance of the interaction of Cho with CRAC or CARC motifs, a potential change in the distribution or orientation of Cho was studied. In this sense, the angle formed by the head-to-tail vector of Cho (considering the O atom and the C20 of the Cho molecule) and the normal of the membrane ( $z$  axis) was calculated for SIII systems (Figure 8B). Results show the presence of two Cho populations either for the SIIIC system or for membranes interacting with peptides: one distributed as the phospholipids, with the OH group near the interphase of POPC and the aliphatic tail in the core of the membrane (with tilt angles of  $\sim 30$  and  $\sim 150^\circ$  in accordance with each monolayer), and other population perpendicular to the normal of the bilayer with angles of  $\sim 90^\circ$ , as shown in Figure 8B,C. In the absence of peptides, Cho is mainly distributed as the phospholipids, with a few molecules perpendicular to the normal of the bilayer. The same effect is observed in membranes interacting with PEP 1. Instead, when PEP 2 interacts with these

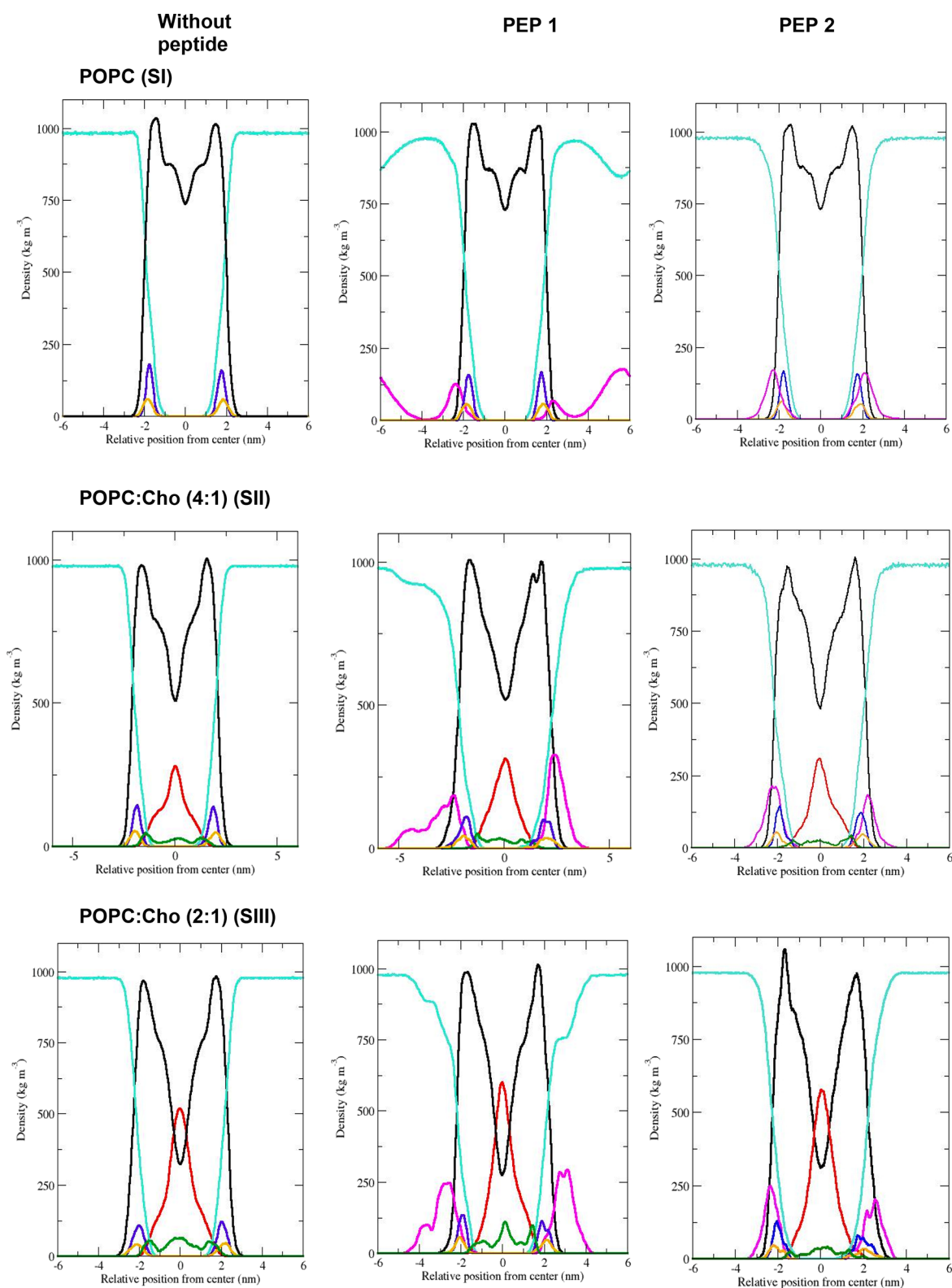


**Figure 7.** Mass density profiles (MDPs) of the different simulated systems. (A) MDP of systems: SIC, SIA, and SIB, respectively. (B) MDP of systems: SIIC, SIIA, and SIIIB, respectively. (C) MDP of systems: SIIC, SIIIA, and SIIIB, respectively. The patterns of colors represent the following: peptide (magenta), Cho (red), OH of Cho (green), POPC (black), phosphate groups of POPC (blue), choline groups of POPC (orange), and water (cyan).

membranes, a significant increase in the Cho population at the center of the membrane is observed.

Figure 8C shows representative snapshots of the peptides interacting with SIII bilayers at the end of simulations ( $t_f = 200$

ns). Images show that PEP 2 interacts and penetrates more into the bilayer compared to PEP 1, the same as the different distribution of Cho molecules in the three SIII systems.



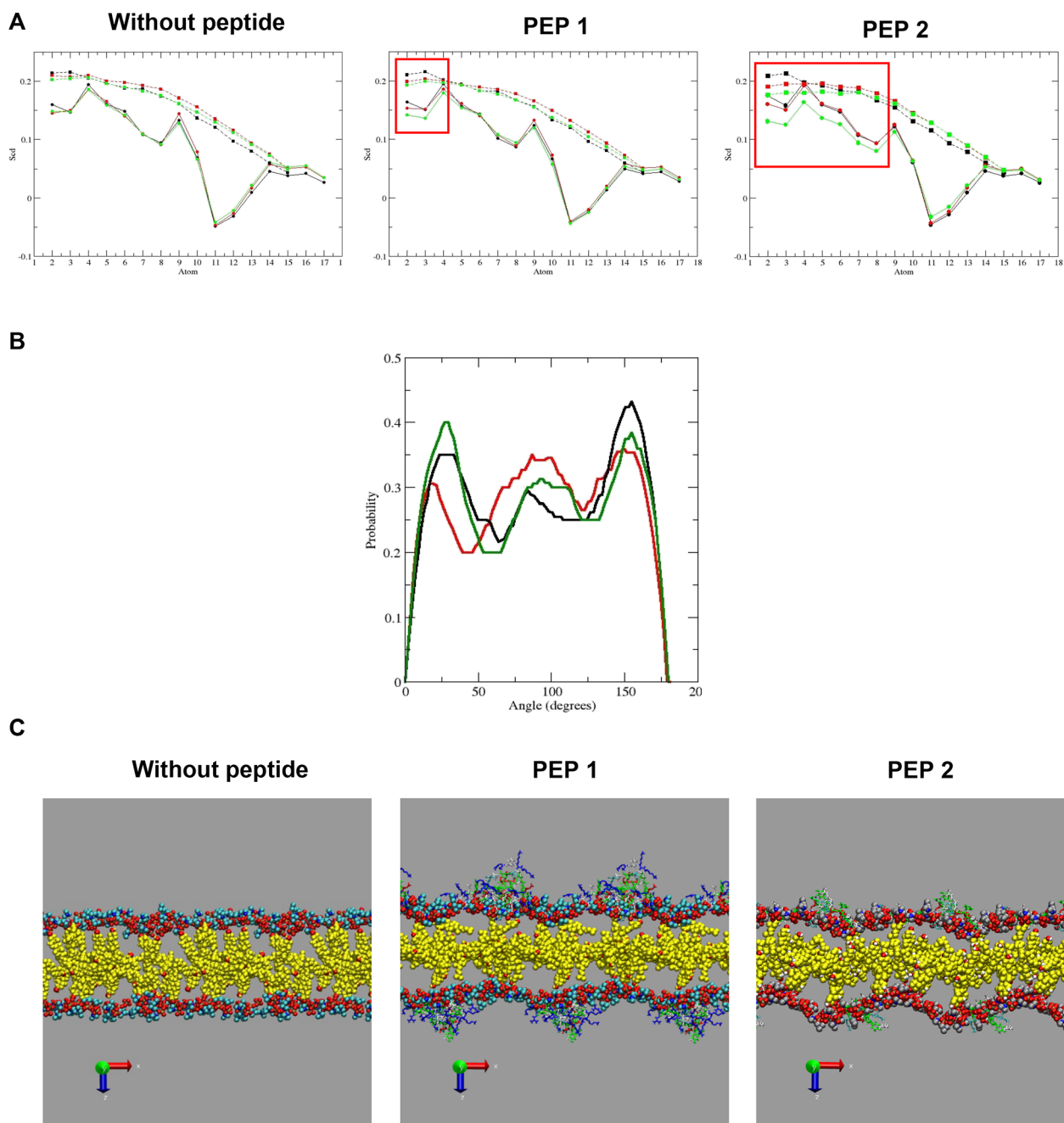


**Figure 8.** Modulation of phospholipid parameters and sterol distribution by the presence of PEP 1 or PEP 2. (A) Order parameter of palmitoyl (dashed lines) and oleoyl (solid line) chains of POPC (SI) (black dots), POPC/Cho (4:1) (SII) (red dots), and POPC/Cho (2:1) (SIII) (green dots) membranes in the absence of peptides (left panel) and in the presence of PEP 1 (middle panel) and PEP 2 (right panel). Red squares indicate the affected carbons in all the systems treated with peptides. (B) Histograms of the angles between the head-to-tail (O-C20) Cho vector and the normal of the membrane during the last 100 ns of the simulation time: SIIIC system (green), SIIIA system (black), SIIIB system (red). (C) Representative snapshots of the final state of SIII systems.  $T_f = 200$  ns. The polar headgroups of POPC (phosphate and choline groups) and Cho are represented as VDW. Peptides are represented in licorice, colored by the polarity of their residues. Water and hydrocarbon tails of POPC are not shown to improve visualization.

Results up to now indicate that PEP 2 presents more affinity than PEP 1 toward Cho-containing membranes. Judging by SPR and MD results, PEP 2 inserts more in membranes containing 33% of Cho and induces a higher perturbation of all the lipids in the membrane compared to PEP 1.

Considering that PEP 2 produces a reorganization of lipids in the membranes, a specific interaction of the peptides with Cho was analyzed. This interaction was studied for both

peptides in the SIII because these were the membranes that presented a greater interaction with each peptide in Figure 6.

Significant interactions are considered when molecules were close enough ( $<10 \text{ \AA}$ ) to Cho for at least 10 ns. Figure 9A shows that 5 of the 10 PEP 1 molecules studied are close to Cho. Otherwise, 7 of the 10 PEP 2 studied are close to the sterol. Each peptide is denoted with a different color. The interaction between PEP 2 and Cho is more stable in time compared to the PEP 1–Cho interaction. This is clearly

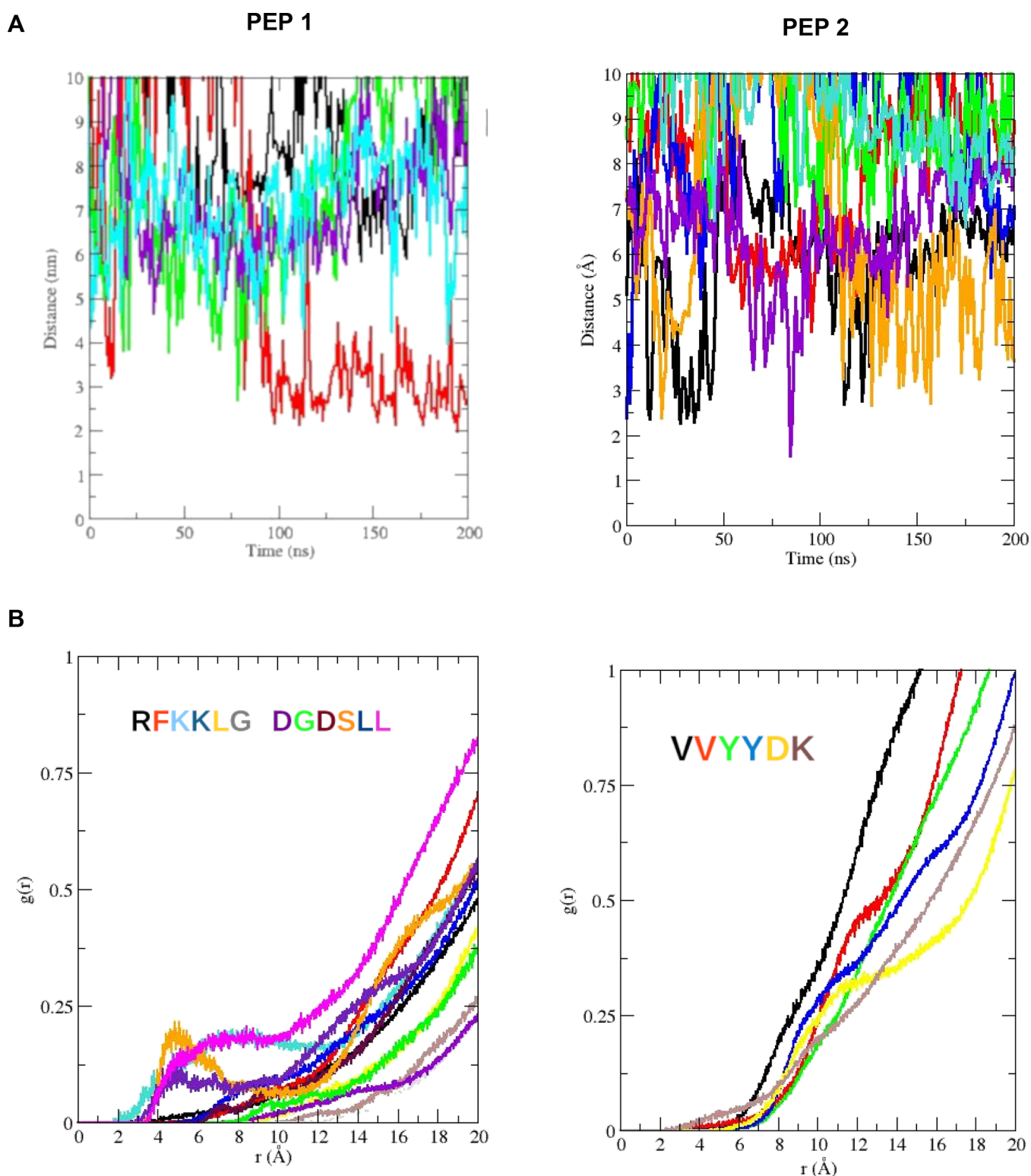


**Figure 9.** Analysis of specific interaction of Cho with PEP 1 and PEP 2. (A) Plot of the distance (up to 10 Å) of the center of mass (COM) of Cho molecules to COM of PEP 1 and PEP 2 in SIII as a function of time. Each peptide is denoted with a different color. (B) Radial distribution functions of COM of Cho molecules to the COM of the different amino acids of PEP 1 and PEP 2. The color of each amino acid is indicated in the sequence of each peptide.

observed, for example, for the red and black PEP 1 molecules where transient interactions are observed; instead, most of PEP 2-Cho interactions last 200 ns.

Taking into account the proximity of the peptides with Cho, we next analyzed whether this interaction was specific for any

of the amino acids. For that purpose, the radial distribution function of the Cho molecules with respect to each one of the amino acid residues of the peptide molecules that presented proximity to Cho (Figure 9B) was analyzed. No specific interaction between Cho and any of the amino acids of PEP 2

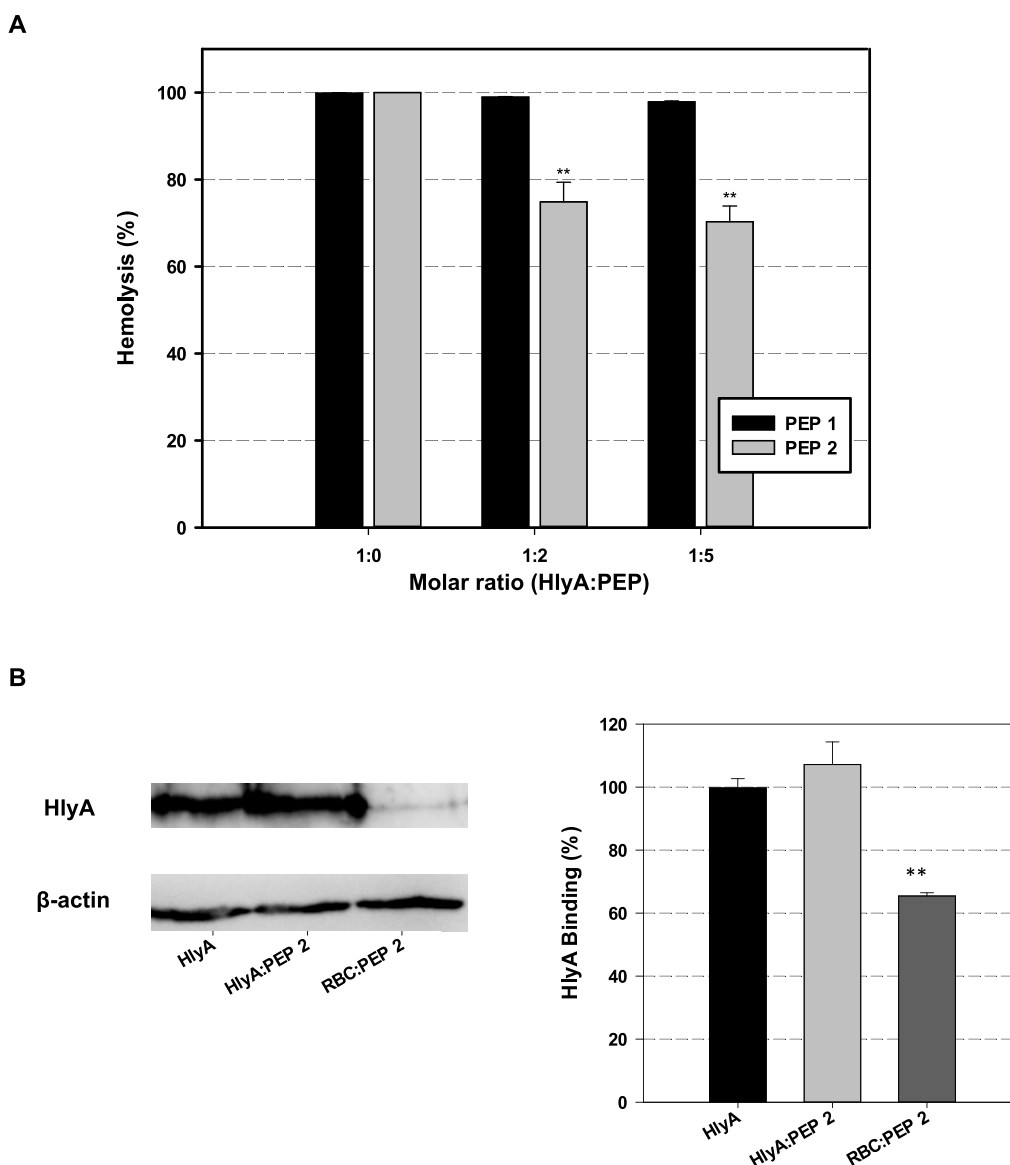


**Figure 10.** Inhibition of HlyA lytic activity by PEP 1 and PEP 2. (A) Hemolysis percentage of 2% v/v erythrocytes as a function of different toxin/peptide molar ratios. Black bars correspond to erythrocytes preincubated with PEP 1, and gray bars correspond to erythrocytes preincubated with PEP 2 ( $N = 3$ ). (B) Left panel: Western blot membranes of ghost erythrocytes treated with HlyA (20  $\mu\text{g}$ ), HlyA/PEP 2, and erythrocytes/PEP 2. The HlyA/PEP 2 molar ratio was 1:5 in both cases. Membranes were developed with anti-HlyA antibodies (first row) and with anti  $\beta$ -actin antibodies (second row) ( $N = 2$ ). Right panel: The binding percentage of HlyA was calculated as the optical density ratio between HlyA and  $\beta$ -actin bands.

is detected; all the amino acids are close enough to Cho molecules at less than 7 Å. Instead, only some of the amino acids located at the N- and C- terminal ends of PEP 1 interact specifically with Cho. Probably, the nature of the amino acids and the shorter length of PEP 2 compared to PEP 1 facilitate peptide insertion and interaction with the membrane, causing a distribution of Cho.

**Inhibition of HlyA Hemolytic Activity by PEP 1 and PEP 2.** Results up to now indicate that PEP 2 interacts preferentially with Cho-containing membranes (Figures 6–8) and that all amino acids of this peptide seem to be close to Cho in the membrane (Figure 9), suggesting that this CRAC sequence in HlyA might facilitate toxin interaction with this sterol. But results are not very conclusive regarding whether both peptides interact specifically with Cho, thus indicating that these sequences might act as CRAC and CARC sites in

the toxin. Then, our hypothesis is that because the toxin needs to interact with Cho to lyse erythrocytes, the preincubation of these cells with the peptides might diminish the activity of the toxin if the peptides interact with Cho. So, the hemolytic activity of the toxin in the presence of increasing amounts of peptides (Figure 10A) was assayed. Results indicate that PEP 2 inhibits toxin hemolytic activity as the amount of peptide increases. It produces 30% of inhibition for a molar ratio toxin/peptide of 1:5. Instead, PEP 1 does not affect the toxin activity at any of the molar ratios tested, probably because it is not so deeply localized in the membrane as PEP 2.

To further investigate whether PEP 2 affects HlyA–membrane interaction, the binding percentage of HlyA to ghost erythrocytes in the presence and absence of PEP 2 was analyzed by Western blot. The binding percentage was calculated as the ratio between the optical density of HlyA



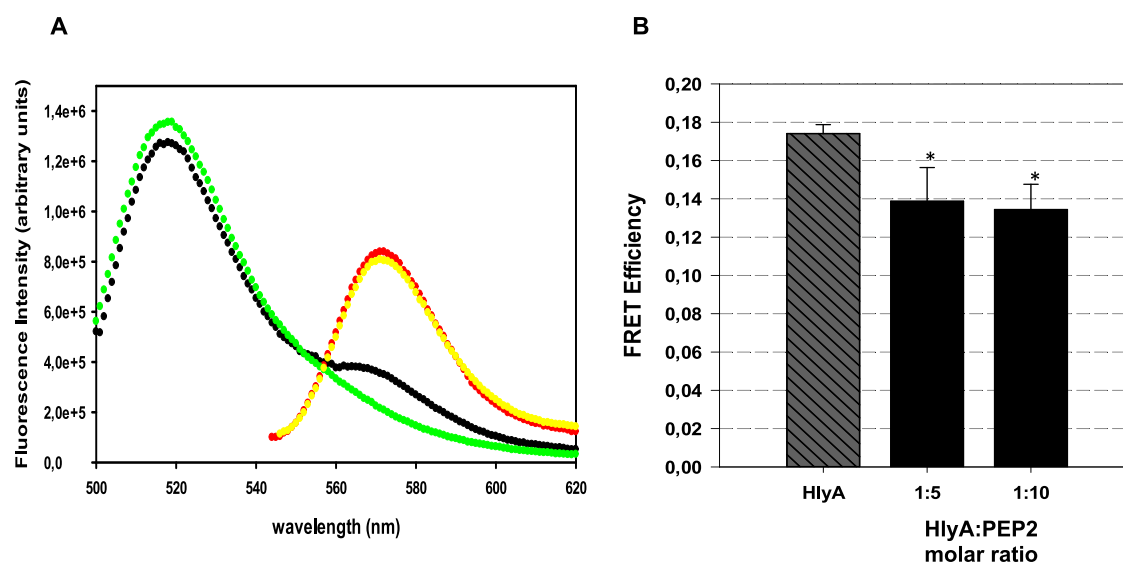


**Figure 11.** PEP 2 inhibits toxin oligomerization. (A) An example of the spectra measured for FRET experiments. The fluorescence emission spectrum of ghost erythrocytes containing D/A excited at 480 nm ( $\lambda_{\text{exc}}=480$ ) is in black, the spectrum of HlyA labeled only with donor bound to ghost excited at 480 nm ( $\lambda_{\text{exc}}=480$ ) is in green, the spectrum of ghost containing D/A excited at 530 nm ( $\lambda_{\text{exc}}=530$ ) is in red, and the emission spectrum of HlyA labeled only with acceptor bound to erythrocyte ghosts ( $\lambda_{\text{exc}}=480$ ) is in yellow. (B) FRET efficiency plotted against HlyA (dashed gray bar) and HlyA/PEP 2 molar ratios 1:5 and 1:10 (black bars) ( $N = 2$ ).

and  $\beta$ -actin bands, assuming that HlyA (in the absence of peptide) was bound by 100%. The blot image and bar plot (Figure 10B) show that HlyA binding to membranes is inhibited when PEP 2 is preincubated with RBC membranes. Another preincubating approach was also tested. In this case, first, HlyA was preincubated with PEP 2 at a molar ratio 1:5, and then, erythrocyte ghosts were added. Figure 10B shows that when HlyA is preincubated with PEP 2, the binding percentage of the toxin to membranes does not diminish, discarding a potential interaction between the toxin and the peptide that might affect the binding of the toxin to the membrane.

**Inhibition of HlyA Oligomerization in the Presence of PEP 2.** Previously, we have demonstrated that HlyA oligomerizes in erythrocyte membranes to form pores that finally lead to hemolysis and that this is a Cho-dependent process.<sup>8</sup> Therefore, the oligomerization process of HlyA was also studied in the presence of PEP 2 by fluorescence resonance energy transfer (FRET) measurements. The distance over which energy can be transferred depends on the spectral characteristics of the fluorophores, but it is generally in the 10–100 Å range. Hence, FRET can be used for measuring the interaction between molecules.<sup>50</sup>

To carry out this assay, a single mutant toxin (HlyA K344C) was used. The purpose of this was to introduce a single cysteine residue to the toxin to ensure the single labeling with a maleimide-derived fluorophore. Two populations of HlyA K344C mutant proteins were used: one labeled with Alexa-488 (donor) and the other one with Alexa-546 (acceptor). Labeled mutant proteins were incubated with erythrocyte membranes (ghosts), and fluorescence was measured. As in the previous assays, erythrocyte ghosts were preincubated with PEP 2.

Figure 11A shows an example of the spectra obtained for the different mixtures that are necessary to calculate  $E$ . On the other hand, Figure 11B shows the FRET efficiency ( $E$ ) for the different HlyA/PEP 2 molar ratios calculated as described in the Materials and Methods section. Results indicate that the presence of PEP 2 significantly diminishes FRET efficiency in a

concentration-dependent manner. The decrease in FRET efficiency indicates a decrease in HlyA oligomerization. This result agrees with the decrease observed in toxin-binding and hemolytic activity inhibition (Figure 10).

Knowing that oligomerization of HlyA is facilitated by the Cho of membranes,<sup>8</sup> this result tempts us to speculate that PEP 2 might block the interaction of the toxin with Cho, which facilitates toxin oligomerization.

## DISCUSSION

The herein presented results show that two peptides whose sequence corresponds to a CARC region situated in the insertion domain of HlyA (PEP 1) and to a CRAC region situated between the acylated-K (PEP 2) interact more strongly with Cho-containing membranes than with pure POPC. The latter presents more affinity for these membranes than PEP 1. Judging from the molecular dynamics studies, PEP 2 inserts and distorts the membrane more than the other peptide. Even more, it inhibits HlyA hemolytic activity.

The previous results that led us to propose the present work indicated that HlyA is less active in Cho-depleted RBC, suggesting that the presence of this sterol in membranes is important for the hemolytic process.<sup>8</sup> Furthermore, we demonstrated that HlyA and its inactive counterpart ProHlyA are associated with detergent-resistant membrane domains (DRMs).<sup>8</sup> These entities are membrane microdomains enriched in sphingomyelin and Cho. The fact that ProHlyA colocalizes with HlyA and flotillin in DRMs suggests that the saturated acyl chains covalently bound to the toxin are not responsible for the partition of the protein in these microdomains, as it was proposed for other proteins.<sup>51</sup> It was suggested that along with the post-translational acylation of proteins, the presence of amino acid sequences in their structure that bind certain lipid components can determine the distribution of proteins into membrane domains enriched with such components. The CRAC motif was considered as such amino acid sequence.<sup>52</sup>

Taking all these into account and considering our results that demonstrate that PEP 2 presents a lower  $K_D$  in its interaction with membranes containing Cho than pure POPC and that it inhibits HlyA binding to the membrane, we are tempted to propose that this CRAC region participates in the interaction with Cho, favoring the insertion of the toxin into the membrane in the adequate conformation to promote toxin oligomerization. Furthermore, MD simulation demonstrated that amino acids of this region are located close to Cho, inducing a distribution of the sterol in the membrane, an effect that was not observed for PEP 1.

Previously, we demonstrated that HlyA presents a molten globule conformation in solution and that its inactive counterpart, ProHlyA, presents a more compact structure.<sup>21</sup> Our hypothesis was that the presence of fatty acids covalently bound to the toxin favored this molten globule conformation, exposing intrinsically disordered regions important in the mechanism of action of the toxin.<sup>21</sup> In view of the results obtained by Ludwig *et al.*<sup>45</sup> and Pellet and Welch,<sup>43</sup> who demonstrated that the hemolytic and cytotoxic activities of the deletion mutants (HlyA  $\Delta 622$ –657 and HlyA  $\Delta 623$ –673) are inactive, together with the results obtained in the present work, we are tempted to speculate that the CRAC region between the acylated sites might be exposed to interact with Cho and in this way favors the insertion of the toxin in the membrane. Other results previously published by us that support this hypothesis are those obtained by polarization-modulated infrared reflection-absorption spectroscopy (PM-IRRAS) experiments, which were performed at the air–water interface, and lipid monolayers mimicking the outer leaflet of erythrocytes membranes.<sup>10</sup> Results obtained in the present work suggest that the presence of the fatty-acyl moieties favors the kinetics of association of the protein, exposing critical domains of HlyA when located at the interface. This could play a relevant role in the stable anchoring and toxic activity of the protein by facilitating protein–protein interactions between toxin monomers and/or membrane receptors.

Recently, we measured the  $K_D$  between HlyA and liposomes composed by POPC, sphingomyelin, and Cho, and its value ( $1.5 \times 10^{-5}$  M) is in the order of magnitude of the ones measured in the present work.<sup>24</sup> This implicates that the interaction of this CRAC region might be the responsible for the irreversible binding of the toxin to membranes.<sup>53</sup>

Regarding the specific interaction of PEP 1 with Cho, results are not very conclusive. Although there is a decrease in the  $K_D$  values for membranes containing Cho with respect to pure POPC, the fact that it does not inhibit toxin activity gives an idea that the interaction of this CARC site with the membrane is not so relevant in the mechanism of action of the toxin. Furthermore, MD results indicate that this peptide does not alter lipid distribution in the membrane as PEP 2. Many authors conclude that the presence of the CRAC or CARC motif in a primary structure of a protein or peptide is not an exclusive criterion for its preferential interaction or binding with Cho. CRAC containing peptides or protein regions can either bind or not to the sterol. In addition, Cho can bind to peptides or protein regions that lack these motifs.<sup>54,55</sup>

The main result obtained in this work is the inhibitory effect CRAC peptide has on the hemolytic process of HlyA. It produces almost 30% of inhibition at a molar ratio toxin/peptide of 1:5 when preincubation with erythrocytes takes place. This finding supports the hypothesis that this CRAC region interacts with Cho. Even more, the fact that this

inhibition is due to a decrease in the binding of the toxin to the membrane confirms this hypothesis. This decrease in the binding of the toxin to the membrane is also reflected in a decrease in the oligomerization of the toxin.

On the other hand, the fact that this CRAC peptide inhibits toxin hemolytic activity tempts us to develop a new medical treatment against the uropathogenic strains of *E. coli*, especially for those treatments in which antibiotic therapy is contraindicated, for instance, in pregnant women. Furthermore, the implementation of new and alternative therapies is necessary because of the increase in antibiotic-resistant strains of *E. coli*.<sup>56,57</sup> The potential of antitoxin strategies is immense, as these peptides provide specific, targeted activity and would not produce the negative side effects associated with traditional antibiotics.<sup>58</sup> Additionally, these approaches would also protect the host microbiota, affecting only the pathogenic bacteria.

The fact that this peptide might inhibit any other toxin, which might need to interact with cholesterol to induce damage, is even more interesting. It is such the case for cholesterol-binding cytolysins, a large family of pore-forming toxins that are secreted by many species of Gram-positive bacteria.<sup>59</sup> There also exists the possibility to inhibit other toxins of the RTX family, such as leukotoxin (LtxA) produced by *Aggregatibacter actinomycetemcomitans*. Brown *et al.* have also found a CRAC peptide that inhibits its activity,<sup>60</sup> so it would be very interesting to check whether both peptides inhibit both toxins.

## CONCLUSIONS

Considering that HlyA needs Cho to oligomerize<sup>8</sup> and that fatty acids covalently bound to the toxin are necessary to expose critical regions involved in the mechanism of action of the toxin,<sup>21</sup> our results indicate that one critical region might be the CRAC site situated strategically between both acylated lysines. The binding of the toxin to Cho, through this site, might induce its insertion into the membrane in an adequate conformation that promotes oligomerization of the toxin, inducing membrane destabilization and/or calcium influx.<sup>61</sup> The fact that a peptide derived from this CRAC moiety inhibits toxin activity leads us into the design of alternative therapies to treat infections induced by uropathogenic strains of *E. coli*.

On the other hand, the finding that a CARC-derived peptide from the insertion domain does not inhibit toxin activity implicates that its binding to Cho is not critical for the mechanism of action of the toxin.

## AUTHOR INFORMATION

### Corresponding Author

Vanesa Herlax – CCT-La Plata, CONICET, Facultad de Ciencias Médicas, Universidad Nacional de La Plata, Instituto de Investigaciones Bioquímicas de La Plata (INIBIOLP), La Plata 1900, Argentina; [orcid.org/0000-0003-4218-8702](https://orcid.org/0000-0003-4218-8702); Phone: 54-221-482-4894; Email: [vherlax@med.unlp.edu.ar](mailto:vherlax@med.unlp.edu.ar); Fax: 54-221-4258988

### Authors

Lucía Cané – CCT-La Plata, CONICET, Facultad de Ciencias Médicas, Universidad Nacional de La Plata, Instituto de Investigaciones Bioquímicas de La Plata (INIBIOLP), La Plata 1900, Argentina; [orcid.org/0000-0003-4356-6429](https://orcid.org/0000-0003-4356-6429)

Fanny Guzmán – Núcleo de Biotecnología Curauma (NBC), Pontificia Universidad Católica de Valparaíso, Valparaíso 2373223, Chile

Galo Balatti – Departamento de Ciencia y Tecnología, Universidad Nacional de Quilmes, Universidad de Buenos Aires, Consejo Nacional de Investigaciones Científicas y Técnicas (CONICET), Buenos Aires 1876, Argentina; Universidad de Buenos Aires, Consejo Nacional de Investigaciones Científicas y Técnicas (CONICET), Instituto de Química y Metabolismo del Fármaco (IQUIMEFA), Buenos Aires 1113, Argentina; [orcid.org/0000-0003-1900-1188](https://orcid.org/0000-0003-1900-1188)

María Antonieta Daza Millone – CCT-La Plata, CONICET. Universidad Nacional de La Plata, Instituto de Investigaciones Físicoquímicas Teóricas y Aplicadas (INIFTA), La Plata 1900, Argentina; [orcid.org/0000-0002-4227-5868](https://orcid.org/0000-0002-4227-5868)

Melisa Pucci Molineris – CCT-La Plata, CONICET, Facultad de Ciencias Médicas, Universidad Nacional de La Plata, Instituto de Investigaciones Bioquímicas de La Plata (INIBIOLP), La Plata 1900, Argentina; [orcid.org/0000-0002-2959-7571](https://orcid.org/0000-0002-2959-7571)

Sabina Maté – CCT-La Plata, CONICET, Facultad de Ciencias Médicas, Universidad Nacional de La Plata, Instituto de Investigaciones Bioquímicas de La Plata (INIBIOLP), La Plata 1900, Argentina

M. Florencia Martini – Universidad de Buenos Aires, Consejo Nacional de Investigaciones Científicas y Técnicas (CONICET), Instituto de Química y Metabolismo del Fármaco (IQUIMEFA), Buenos Aires 1113, Argentina; Cátedra de Química Medicinal, Facultad de Farmacia y Bioquímica, Universidad de Buenos Aires, Buenos Aires 1113, Argentina; [orcid.org/0000-0002-1949-9310](https://orcid.org/0000-0002-1949-9310)

Complete contact information is available at:

<https://pubs.acs.org/10.1021/acs.biochem.3c00164>

## Notes

The authors declare no competing financial interest.

## ACKNOWLEDGMENTS

V.H., S.M., M.A.D.M., and M.F.M. are established researchers of the Carrera del Investigador of Consejo Nacional de Investigación en Ciencia y Tecnología (CONICET). M.F.M. and G.E.B. thank Sistema Nacional de Cómputos (SNCAD-CONICET) and Centro de Computación de Alto Desempeño de la Universidad de Córdoba (CCAD-UNC) for the computational resources used. Mrs. Rosana del Cid, a professional translator, edited the final version of the manuscript. This work was supported by the Agencia Nacional de Promoción Científica y Tecnológica [Grant PICT 2017-2393] and Universidad Nacional de La Plata (UNLP) [Grant M225].

## ABBREVIATIONS

CD:circular dichroism; Cho:cholesterol; CRAC:cholesterol recognition/amino acid consensus; DCM:dichloromethane; DIEA:*N,N*-diisopropylethylamine; DMF:*N,N*-dimethylformamide; DTT:dithiothreitol; HBTU:(*N*-[(1*H*-benzotriazol-1-yl)-(dimethylamino) methylene]-*N*-methylmethanaminium hexafluorophosphate *N*-oxide; HlyA:alpha hemolysin of *Escherichia coli*; IPA:isopropyl alcohol;  $K_D$ :dissociation constant; MD:molecular dynamics; MLVs:multilamellar vesicles;

MTT:3-(4,5-dimethylthiazol-2-yl)-2,5-diphenyltetrazolium bromide; PBS:phosphate-buffered saline; POPC:1-palmitoyl-2-oleoyl-glycero-3-phosphocholine; RBC:erythrocytes; RTX:“Repeat in Toxins”; SLB:supported lipid bilayer; SPPS:solid-phase peptide synthesis; SPR:surface plasmon resonance; SUVs:small unilamellar vesicles; TBTU:(2-(1*H*-benzotriazol-1-yl)-1,1,3,3-tetramethyluronium hexafluorophosphate; TC:20 mM Tris and 150 mM NaCl, pH = 7,4; TFA:trifluoroacetic acid; TFE:2,2,2-trifluoroethanol; TIR:total internal reflection; UPEC:uropathogenic strains of *Escherichia coli*; UTIs:urinary tract infections

## REFERENCES

- (1) Foxman, B.; Brown, P. Epidemiology of urinary tract infections: transmission and risk factors, incidence, and costs. *Infect. Dis. Clin. North Am.* **2003**, *17*, 227–241.
- (2) Wiles, T. J.; Kulesus, R. R.; Mulvey, M. A. Origins and virulence mechanisms of uropathogenic *Escherichia coli*. *Exp. Mol. Pathol.* **2008**, *85*, 11–19.
- (3) Marrs, C. F.; Zhang, L.; Foxman, B. *Escherichia coli* mediated urinary tract infections: are there distinct uropathogenic *E. coli* (UPEC) pathotypes? *FEMS Microbiol. Lett.* **2005**, *252*, 183–190.
- (4) Cavalieri, S.; Bohach, G. A.; Synder, I. *Escherichia coli* alpha-hemolysin characteristics and probable role in pathogenicity. *Microbiol. Rev.* **1984**, *48*, 326–343.
- (5) Issartel, J.-P.; Koronakis, V.; Hughes, C. Activation of *Escherichia coli* prohaemolysin to the mature toxin by acyl carrier protein-dependent fatty acylation. *Nature* **1991**, *351*, 759–761.
- (6) Stanley, P.; Packman, L. C.; Koronakis, V.; Hughes, C. Fatty acylation of two internal lysine residues required for the toxic activity of *Escherichia coli* hemolysin. *Science* **1994**, *266*, 1992–1996.
- (7) Stanley, P.; Koronakis, V.; Hughes, C. Acylation of *Escherichia coli* hemolysin: A unique protein lipidation mechanism underlying toxin function. *Microbiol. Mol. Biol. Rev.* **1998**, *62*, 309–333.
- (8) Herlax, V.; Mate, S.; Rimoldi, O.; Bakas, L. Relevance of fatty acid covalently bound to *Escherichia coli* alpha-hemolysin and membrane microdomains in the oligomerization process. *J. Biol. Chem.* **2009**, *284*, 25199–25210.
- (9) Sanchez-Magraner, L.; Cortajarena, A.; Goni, F.; Ostolaza, H. Membrane insertion of *Escherichia coli* alpha-hemolysin is independent from membrane lysis. *J. Biol. Chem.* **2006**, *281*, 5461–5467.
- (10) Vazquez, R. F.; Millone, M. A. D.; Pavinatto, F. J.; Herlax, V. S.; Bakas, L. S.; Oliveira, O. N., Jr.; Vela, M. E.; Mate, S. M. Interaction of acylated and unacylated forms of *E. coli* alpha-hemolysin with lipid monolayers: a PM-IRRAS study. *Colloids Surf., B* **2017**, *158*, 76–83.
- (11) Vazquez, R. F.; Mate, S. M.; Bakas, L. S.; Munoz-Garay, C.; Herlax, V. S. Relationship between intracellular calcium and morphological changes in rabbit erythrocytes: Effects of the acylated and unacylated forms of *E. coli* alpha-hemolysin. *Biochim. Biophys. Acta* **2016**, *1858*, 1944–1953.
- (12) Cavalieri, S. J.; Snyder, I. S. Effect of *Escherichia coli* alpha-hemolysin on human peripheral leukocyte viability *in vitro*. *Infect. Immun.* **1982**, *36*, 455–461.
- (13) Bhakdi, S.; Muhly, M.; Korom, S.; Schmidt, G. Effects of *Escherichia coli* hemolysin on human monocytes. Cytocidal action and stimulation of interleukin I release. *J. Clin. Invest.* **1990**, *85*, 1746–1753.
- (14) Welch, R. RTX Toxin Structure and Function: A Story of Numerous Anomalies and Few Analogies in Toxin Biology. *Curr. Top Microbiol Immunol* **2001**, *257*, 85–111.
- (15) Strack, K.; Lauri, N.; Maté, S. M.; Saralegui, A.; Muñoz-Garay, C.; Schwarzbaum, P. J.; Herlax, V. Induction of erythrocyte microvesicles by *Escherichia Coli* Alpha hemolysin. *Biochem. J.* **2019**, *476*, 3455–3473.
- (16) Ostolaza, H.; Bartolome, B.; de Zarate, I. O.; de la Cruz, F.; Goñi, F. M. Release of lipid vesicle contents by the bacterial protein toxin alpha-haemolysin. *Biochim. Biophys. Acta* **1993**, *1147*, 81–88.



- (17) Bakás, L.; Ostolaza, H.; Vaz, W. L.; Goñi, F. M. Reversible adsorption and nonreversible insertion of *Escherichia coli* alpha-hemolysin into lipid bilayers. *Biophys. J.* **1996**, *71*, 1869–1876.
- (18) Bakás, L.; Veiga, M.; Soloaga, A.; Ostolaza, H.; Goñi, F. Calcium-dependent conformation of *E. coli* alpha-hemolysin. Implications for the mechanism of membrane insertion and lysis. *Biochim. Biophys. Acta* **1998**, *1368*, 225–234.
- (19) Bakás, L.; Maté, S.; Vazquez, R.; Herlax, V. *E. coli* Alpha Hemolysin and properties, in *Biochemistry*, Book, I, P.D., Ekinci, Editor: Croacia 2012.
- (20) Hyland, C.; Vuillard, L.; Hughes, C.; Koronakis, V. Membrane interaction of *Escherichia coli* Hemolysin: Flotation and Insertion-Dependent Labeling by Phospholipid Vesicles. *J. Bacteriol.* **2001**, *183*, 5364–5370.
- (21) Herlax, V.; Bakas, L. Fatty acids covalently bound to alpha-hemolysin of *Escherichia coli* are involved in the molten globule conformation: implication of disordered regions in binding promiscuity. *Biochemistry* **2007**, *46*, 5177–5184.
- (22) Bakas, L.; Chanturiya, A.; Herlax, V.; Zimmerberg, J. Paradoxical lipid dependence of pores formed by the *Escherichia coli* alpha-hemolysin in planar phospholipid bilayer membranes. *Biophys. J.* **2006**, *91*, 3748–3755.
- (23) Moayeri, M.; Welch, R. Effects of temperature, time, and toxin concentration on lesion formation by the *Escherichia coli* hemolysin. *Infect. Immun.* **1994**, *62*, 4124–4134.
- (24) Vazquez, R. F.; Maté, S. M.; Bakás, L. S.; Fernández, M. M.; Malchiodi, E. L.; Herlax, V. S. Novel evidence for the specific interaction between cholesterol and an RTX toxin. *Biochem. J.* **2014**, *458*, 481–489.
- (25) Li, H.; Papadopoulos, V. Peripheral-type benzodiazepine receptor function in cholesterol transport. Identification of a putative cholesterol recognition/interaction amino acid sequence and consensus pattern. *Endocrinology* **1998**, *139*, 4991–4997.
- (26) Baier, C. J.; Fantini, J.; Barrantes, F. J. Disclosure of cholesterol recognition motifs in transmembrane domains of the human nicotinic acetylcholine receptor. *Sci. Rep.* **2011**, *1*, 0069.
- (27) Fantini, J.; Di Scala, C.; Baier, C. J.; Barrantes, F. J. Molecular mechanisms of protein-cholesterol interactions in plasma membranes: Functional distinction between topological (tilted) and consensus (CARC/CRAC) domains. *Chem. Phys. Lipids* **2016**, *199*, 52–60.
- (28) Brown, A. C.; Balashova, N. V.; Epand, R. M.; Epand, R. F.; Bragin, A.; Kachlany, S. C.; Walters, M. J.; Du, Y.; Boesze-Battaglia, K.; Lally, E. T. *Aggregatibacter actinomycetemcomitans* leukotoxin utilizes a cholesterol recognition/amino acid consensus site for membrane association. *J. Biol. Chem.* **2013**, *288*, 23607–23621.
- (29) Daza Millone, M. A.; Vázquez, R. F.; Maté, S. M.; Vela, M. E. Phase-segregated Membrane Model assessed by a combined SPR-AFM Approach. *Colloids Surf., B* **2018**, *172*, 423–429.
- (30) Creczynski-Pasa, T. B.; Millone, M. A. D.; Munford, M. L.; de Lima, V. R.; Vieira, T. O.; Benitez, G. A.; Pasa, A. A.; Salvarezza, R. C.; Vela, M. E. Self-assembled dithiothreitol on Au surfaces for biological applications: phospholipid bilayer formation. *Phys. Chem. Chem. Phys.* **2009**, *11*, 1077–1084.
- (31) Papo, N.; Shai, Y. Exploring Peptide Membrane Interaction Using Surface Plasmon Resonance: Differentiation between Pore Formation versus Membrane Disruption by Lytic Peptides. *Biochemistry* **2003**, *42*, 458–466.
- (32) Abraham, M. J.; Murtola, T.; Schulz, R.; Páll, S.; Smith, J. C.; Hess, B.; Lindahl, E. GROMACS: High performance molecular simulations through multi-level parallelism from laptops to supercomputers. *SoftwareX* **2015**, *1-2*, 19–25.
- (33) Berendsen, H.; Postma, J. P. M.; van Gunsteren, W.; Hermans, J. Interaction Models for Water in Relation to Protein Hydration, in *Intermolecular Forces. The Jerusalem Symposia on Quantum Chemistry and Biochemistry*, Pullman, B., Editor. 1981, Springer: Dordrecht. p. 331–342.
- (34) Abraham, M. J.; van der Spoel, D.; Lindahl, E.; Hess, B. A.; T. G. D. team., *GROMACS User Manual version 2016*, [www.gromacs.org](http://www.gromacs.org). 2018.
- (35) Van Der Spoel, D.; Lindahl, E.; Hess, B.; Groenhof, G.; Mark, A. E.; Berendsen, H. J. C. GROMACS: fast, flexible, and free. *J. Comput. Chem.* **2005**, *26*, 1701–1718.
- (36) Lindahl, E.; Hess, B.; van der Spoel, D. GROMACS 3.0: a package for molecular simulation and trajectory analysis. *Mol. Model. Annu.* **2001**, *7*, 306–317.
- (37) Berger, O.; Edholm, O.; Jähnig, F. Molecular dynamics simulations of a fluid bilayer of dipalmitoylphosphatidylcholine at full hydration, constant pressure, and constant temperature. *Biophys. J.* **1997**, *72*, 2002–2013.
- (38) Jumper, J.; Evans, R.; Pritzel, A.; Green, T.; Figurnov, M.; Ronneberger, O.; Tunyasuvunakool, K.; Bates, R.; Židek, A.; Potapenko, A.; Bridgland, A.; Meyer, C.; Kohli, S. A. A.; Ballard, A. J.; Cowie, A.; Romera-Paredes, B.; Nikolov, S.; Jain, R.; Adler, J.; Back, T.; Petersen, S.; Reiman, D.; Clancy, E.; Zielinski, M.; Steinegger, M.; Pacholska, M.; Berghammer, T.; Bodenstein, S.; Silver, D.; Vinyals, O.; Senior, A. W.; Kavukcuoglu, K.; Kohli, P.; Hassabis, D. Highly accurate protein structure prediction with AlphaFold. *Nature* **2021**, *596*, 583–589.
- (39) Darden, T.; York, D.; Pedersen, L. Particle mesh Ewald: An Nlog(N) method for Ewald sums in large systems. *J. Chem. Phys.* **1993**, *98*, 10089–10092.
- (40) Essmann, U.; Perera, L.; Berkowitz, M. L.; Darden, T.; Lee, H.; Pedersen, L. G. A smooth particle mesh Ewald method. *J. Chem. Phys.* **1995**, *103*, 8577–8593.
- (41) Humphrey, W.; Dalke, A.; Schulten, K. VMD: visual molecular dynamics. *J. Mol. Graph.* **1996**, *14*, 33–38.
- (42) Moayeri, M.; Welch, R. Prolytic and lytic Conformation of erythrocyte-associated *Escherichia coli* hemolysin. *Infect. Immun.* **1997**, *65*, 2233–2239.
- (43) Pellett, S.; Welch, R. A. *Escherichia coli* hemolysin mutants with altered target cell specificity. *Infect. Immun.* **1996**, *64*, 3081–3087.
- (44) Gohlke, C.; Murchie, A. I. H.; Lilley, D. M. J.; Clegg, R. M. Binding of DNA and RNA helices by bulged nucleotides observed by fluorescence resonance energy transfer. *Proc. Natl. Acad. Sci.* **1994**, *11660*–11664.
- (45) Ludwig, A.; Vogel, M.; Goebel, W. Mutations affecting activity and transport of haemolysin in *Escherichia coli*. *Mol. Gen. Evol.* **1987**, *206*, 238–245.
- (46) Guzmán, F.; Gauna, A.; Roman, T.; Luna, O.; Álvarez, C.; Pareja-Barrueto, C.; Mercado, L.; Albericio, F.; Cárdenas, C. Tea Bags for Fmoc Solid-Phase Peptide Synthesis: An Example of Circular Economy. *Molecules* **2021**, *26*, DOI: 10.3390/molecules26165035.
- (47) Chebre, R.; Leonar, S.; de Brever, A.; Gell, J. PolyprOnline: polyproline helix II and secondary structure assignment database. *Database* **2014**, *2014*, 1–8.
- (48) Thompson, J. D.; Higgins, D. G.; Gibson, T. J. CLUSTAL W: improving the sensitivity of progressive multiple sequence alignment through sequence weighting, position-specific gap penalties and weight matrix choice. *Nucleic Acids Res.* **1994**, *22*, 4673–4680.
- (49) Waterhouse, A. M.; Procter, J. B.; Martin, D. M.; Clamp, A. M.; Barton, G. J. Jalview Version 2—a multiple sequence alignment editor and analysis workbench. *Bioinformatics* **2009**, *25*, 1189–1191.
- (50) Parsons, M.; Vojnovic, B.; Ameer-Beg, S. Imaging protein-protein interactions in cell motility using fluorescence resonance energy transfer (FRET). *Biochem. Soc. Trans.* **2004**, *32*, 431–433.
- (51) de Planque, M. R.; Killian, J. A. Protein-lipid interactions studied with designed transmembrane peptides: role of hydrophobic matching and interfacial anchoring. *Mol. Membr. Biol.* **2003**, *20*, 271–284.
- (52) de Vries, M.; Herrmann, A.; Veit, M. A cholesterol consensus motif is required for efficient intracellular transport and raft association of a group 2 HA from influenza virus. *Biochem. J.* **2015**, *465*, 305–314.
- (53) Herlax, V.; Bakas, L. Acyl chains are responsible for the irreversibility in the *Escherichia coli* alpha-hemolysin binding to membranes. *Chem. Phys. Lipids* **2003**, *122*, 185–190.
- (54) Palmer, M. Cholesterol and the activity of bacterial toxins. *FEMS Microbiol. Lett.* **2004**, *238*, 281–289.

(55) Volynskya, P. E.; Galimzyanovb, T. R.; Akimovb, S. A. Interaction of Peptides Containing CRAC Motifs with Lipids in Membranes of Various Composition. *Biochemistry* **2021**, *15*, 120–129.

(56) Denoble, A.; Reid, H. W.; Krischak, M.; Rosett, H.; Sachdeva, S.; Weaver, K.; Heine, P. R.; Dotters-Katz, S. Bad bugs: antibiotic-resistant bacteriuria in pregnancy and risk of pyelonephritis. *Am. J. Obstet. Gynecol. MFM* **2022**, *4*, No. 100540.

(57) Shah, C.; Baral, R.; Bartaula, B.; Shrestha, L. Virulence factors of uropathogenic *Escherichia coli* (UPEC) and correlation with antimicrobial resistance. *BMC Microbiol.* **2019**, *19*, 204.

(58) Krueger, E.; Brown, A. C. Inhibition of bacterial toxin recognition of membrane components as an anti-virulence strategy. *J. Biol. Eng.* **2019**, *13*, 4.

(59) Hotze, E. M.; Tweten, R. K. Membrane assembly of the cholesterol-dependent cytolysin pore complex. *Biochim. Biophys. Acta* **2012**, *1818*, 1028–1038.

(60) Brown, A. C.; Koufos, E.; Balashova, N. V.; Boesze-Battaglia, K.; Lally, E. T. Inhibition of LtxA Toxicity by Blocking Cholesterol Binding With Peptides. *Mol. Oral Microbiol.* **2016**, *31*, 94–105.

(61) Velasquez, F. C.; Mate, S.; Bakas, L.; Herlax, V. Induction of eryptosis by low concentrations of *E. coli* alpha-hemolysin. *Biochim. Biophys. Acta* **2015**, *1848*, 2779–2788.